Assessing macrophyte seasonal dynamics using dense time series of medium resolution satellite data

Paolo VILLA[1,*], Monica PINARDI[1,2], Rossano BOLPAGNI[2], Jean-Marc GILLIER[3], Peggy ZINKE[4], Florin NEDELCUȚ[5], Mariano BRESCIANI[1]

[1] *Institute for Electromagnetic Sensing of the Environment, National Research Council, Milan, Italy*

[2] *Department of Chemistry, Life Sciences and Environmental Sustainability, University of Parma, Parma, Italy*

[3] *SNPN, Réserve naturelle du lac de Grand-Lieu, Bouaye, France*

[4] *Norwegian University of Science and Technology, Trondheim, Norway*

[5] *Dunărea de Jos University of Galati, Brăila, Romania*

** corresponding author*

Address: Via Bassini 15, 20133 Milan, Italy

Tel: +39 0223699292

Email: villa.p@irea.cnr.it

Abstract

Thanks to the improved spatial and temporal resolution of new generation Earth Observation missions, such as Landsat 8 and Sentinel-2, the capabilities demonstrated in the last decades by remote sensing in mapping land surface phenology of terrestrial biomes can now be tested in inland water systems.

We assessed the capabilities of dense time series of medium resolution satellite data to deliver information about quantitative macrophyte phenology metrics, focusing on three temperate European shallow lakes with connected wetlands: Mantua lakes system (Italy) Lac de Grand-Lieu (France), and Fundu Mare Island (Romania).

Macrophyte leaf area index (LAI) maps were derived from semi-empirical regression modelling based on the best performing spectral index, with an error level around 0.1 m^2 m^{-2}. Phenology metrics computed from LAI time series using TIMESAT code were used to analyse macrophyte seasonal dynamics across the three study areas in terms of spatial patterns and species-dependent variability for the year 2015. These peculiar dynamicity patterns of autochthonous and allochthonous species were related to the environmental characteristics of each area in terms of ecological, hydrological and meteorological conditions. In addition, the influence of cloud cover thresholding, temporal resolution and missing acquisitions was assessed in terms of phenology timing metrics retrieval, thus providing quantitative information on the expected variability of TIMESAT outputs when time series with reduced resolution are used, i.e. if 16-day time revisit Landsat data were used for retrospective study of macrophyte phenology during the last three decades.

Keywords: Vegetation phenology; LAI; Shallow lakes; Spectral Indices; Sentinel-2; Landsat 8.

1. Introduction

Although much is known about the long-term effect of climate change on the phenology of terrestrial ecosystems (Richardson et al., 2013; Yang et al., 2015), there is little information regarding aquatic ecosystems and even less regarding aquatic plants. Improving the knowledge on macrophyte seasonal changes or phenology is essential in order to investigate ecological drivers and to promote effective programs to recover and conserve aquatic vegetation. Some studies exist that focus on emergent macrophytes (Alahuhta et al., 2011), floating plants (Peeters et al., 2013) and their interaction with submerged macrophytes (Netten et al., 2011; Li et al., 2017). These works are mostly based on existing thematic cartography and *in situ* observations of vegetation cover and biomass, thus not covering spatial and temporal scales that allow transferable if not general conclusions. Large lakes and wetland ecosystems are in fact difficult to survey and consequently few data have been collected to describe temporal dynamics of aquatic vegetation, as stressed recently by Luo et al. (2016). Consistent and spatialized data about key phenological features, e.g. the timing of start and end of growing season, are required to better understand the main drivers of aquatic vegetation seasonal dynamics (Wang et al., 2012; Sletvold and Ågren, 2015). Punctual knowledge of seasonal dynamics is also crucial for understanding the arrangement in space and time of macrophyte communities and functional groups, of competition with other primary producers (Bolpagni et al., 2014; Villa et al., 2015; Zhang et al., 2015), as well as potential impact of invasive species (Wolkovich and Cleland, 2011). Furthermore, natural resource managers and policy makers demand knowledge of phenological dynamics over increasingly large temporal and spatial extents for addressing important issues related to global environmental change (White and Nemani, 2003; Cleland et al., 2007).

Within this frame, remote sensing offers near ideal capabilities in terms of spatial and temporal

resolution, synoptic view and coverage, sensitivity to vegetation features (structural and physiological), regular sampling and operational repeatability (Malthus, 2017). Long-term, consistent satellite data are needed to monitor and quantify intra- and inter-annual trends in vegetation change and seasonality (e.g. Villa et al., 2012; Fensholt et al., 2015). A large corpus of scientific literature on remote sensing of land surface phenology has been built in the last decade, focusing in particular on terrestrial biomes (e.g. Reed et al., 1994; Zhang et al., 2003; Fisher and Mustard, 2007). The majority of these works use satellite data with medium to low resolution, i.e. greater than 1 km pixel size (e.g. Jenkins et al., 2002; Reed, 2006; Fisher et al., 2007). Because of the peculiar characteristics of macrophytes (e.g. background conditions, canopy structures) and of their ecosystems (mostly shallow water bodies, with small surfaces and high heterogeneity in species and growth forms), techniques designed for making use of coarse spatial resolution data and targeted at terrestrial plants are not directly applicable and need to be adapted and/or reparametrized. Some studies for the phenological analysis of macrophytes were made using the 30m spatial resolution of the Landsat constellation sensors (e.g. Hestir et al., 2015; Luo et al., 2016) but the 16-day revisiting time with the problem of cloud cover does not allow sure of fully cover the temporal variability of macrophytes growth.

Sentinel-2 satellite constellation, managed by ESA through the Copernicus initiative, started in July 2017 to provide high quality data at 10-20 m resolution, every 5 days (Drusch et al., 2012). Sentinel-2 data, for their characteristics, can be a powerful tool for monitoring macrophytes and their seasonal dynamics with a level of detail never experienced before.

In this paper, we analyse the capabilities of dense time series (5 to 10 day revisit) of medium resolution (10 to 30 m) satellite data to deliver information about macrophyte phenology metrics. For this purpose, we collected data and run the analysis over three European shallow lakes with connected wetlands, hosting macrophyte communities of floating and emergent species, common

to temperate freshwater ecosystems.

In particular, our objectives are: i) to calibrate a semi-empirical model for deriving macrophyte Leaf Area Index (LAI) time series from satellite spectral reflectance data; ii) to map macrophyte phenology metrics and assess their spatial and species-dependent variability across our study areas; iii) to evaluate the influence of input dataset characteristics, in terms of cloud cover amount, temporal resolution, and missing acquisitions on the key seasonality metrics mapped from satellite.

2. Study areas

The study areas were three shallow freshwater bodies with connected wetlands, hosting macrophyte communities, mainly composed by floating and emergent species. The three areas share a temperate climate and are located in Europe: Mantua lakes system (Italy) is the main study area, where extensive *in situ* data collection was carried out for implementing our analysis; Lac de Grand-Lieu (France), and Fundu Mare Island (Romania) are two additional test site areas, for which less reference information were available.

2.1.Mantua lakes system

The Mantua lakes system is located in the Po river floodplain (northern Italy; 45°10' N, 10°47' E; Figure 1) with a continental climatic regime (Peel et al., 2007). The Superior, Middle and Inferior lakes are semi-artificial lakes created from a meander of the Mincio River that was dammed during the 12th century. The three fluvial-lakes are small (surface < 6 km^2), shallow (average depth 3.5 m), and hypertrophic (chlorophyll-a concentrations up to 100 µg L^{-1}). The Superior Lake maintain a constant water level of 17.5 m a.s.l. due to water discharge regulation by the Vasarone sluice gate and Vasarina gate (Pinardi et al., 2015). Also in the Middle and

Inferior lakes, water level is varying in very narrow range (14.0-14.5 m a.s.l.) for reason of hydraulic safety (e.g. avoid flooding in the historic city center). This system is protected as Natural Regional Park and is part of the World Heritage by UNESCO and is surrounded by two wetlands (Valli del Mincio and Vallazza; VM and VW), which are Sites of Community Importance, Special Protection Areas and Nature Reserves. The Mantua lakes system is characterized by the co-existence of phytoplankton and macrophyte (emergent, submersed, floating-leaved and free-floating) communities of primary producers (Pinardi et al., 2011; Bolpagni et al., 2014; Villa et al., 2015). During the vegetative period (April-October) dense stands of the allochthonous species *Nelumbo nucifera* colonize the Superior Lake, with a minor contribution by native autochthonous species as *Nuphar lutea* and *Trapa natans*. In this lake, also submersed species are widespread, such as *Cerathophyllum demersum*. The Middle Lake hosts monospecific stands of *T. natans* with little spots of *N. lutea* and *Nymphaea alba*. The Inferior Lake mainly hosts small and isolated *T. natans* spots. Recently an invasive and allochthonous species (*Ludwigia hexapetala*) has spread in the littoral zones of the Superior and Middle lakes.

2.2.Lac de Grand-Lieu

Lac de Grand-Lieu is a large, eutrophic and shallow freshwater lake in north-western France (Loire-Atlantique department, 47°05’ N, 1°41’ W; Figure 1), located at about 25 km from the Atlantic coast. It extends over 63 km² during winter when the wet meadows, reed beds, willow and alder groves (*Salix* spp., *Alnus* spp.) are flooded. Water level fluctuations follow the seasonal cycle of precipitations and human water level management. A sluice, downstream of the lake, controls water levels since the early 1960s. In spring, the water level drops by one meter on average with respect to the seasonal maximum. Then, during the summer, sluice gates are locked and water level slowly decreases according to the evaporation, until rainy autumn months; depending on the year, the lake level may drop from 15 to 35 cm between July and October. The

permanently flooded central area (21 km^2), around one meter deep, is partially covered by floating-leaved macrophytes (about 7 km²) dominated by *N. alba* and *N. lutea*. Little beds of *T. natans* and *Nymphoides peltata* extend over 15 to 30 ha (Gillier and Reeber, 2016). Submerged macrophytes have strongly declined since the 1960s (Dupont, 2003; Marion and Marion, 1975; Le Bail, 2008). There are still scattered beds of *Potamogeton* ssp., *Najas marina*, *Chara* spp. in the central part of the lake. As in other nearby wetlands (Haury et al., 2011), invasive allochthonous plants, *L. hexapetala* and *L. peploides*, are widely spread in the channels and on the mudflats on the edge of the central area but now also in a more "terrestrial" form on the wet meadows and on the sparse reed beds.

2.3. Fundu Mare Island

Fundu Mare Island (eastern Romania, 45°11' N, 27°57' E; Figure 1), located in the lower Danube River system, is one of few remaining floodplain islands in a nearly natural state. It is part of the Natural Park Small Wetland of Braila (SWB), which is an internationally important bird protection area and was declared as Nature Reserve in 1994. Fundu Mare Island is the northernmost of seven islands in SWB and covers an area of 1945 ha. About 50% of the area is regarded as aquatic habitat, represented by the two shallow lakes Chiriloaia (300 ha) and Misaila (630 ha) (SWB 2015). The lakes are usually flooded during the spring season, when Danube River hits peak discharge. The water level reduces during the following months, depending on the Danube level, temperature, precipitation, and weir regulation in outlet channels (Zinke et al., 2016).

The climate at FM is warm, humid and continental (Peel et al., 2007). The dominating vegetation types on the island include floodplain forests formed by the riparian species *Salix* spp., *Populus* spp., helophytes (*Phragmites australis*, *Schoenoplectus lacustris*) and aquatic macrophytes, with *N. alba* and *T. natans* as dominant species, sometimes mixed with submerged species (mainly

Potamogeton spp.), and some presence of *N. peltata*. During the last few years, massive willow encroachment (*Salix* spp.) has been observed in some formerly open areas, with negative consequences for fish and birds (Zinke et al., 2016).

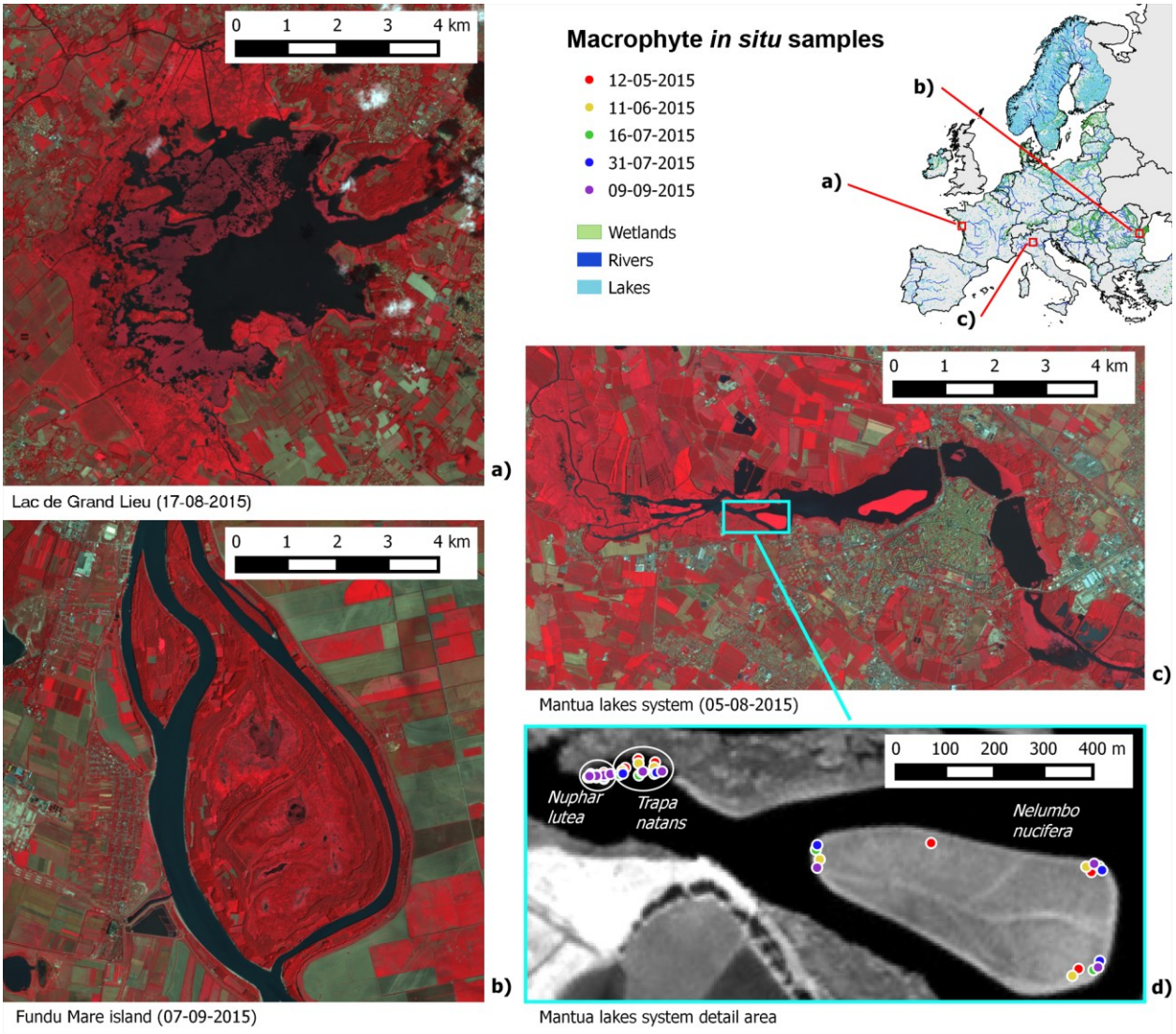

Figure 1. Study areas shown as SPOT5 images in colour infrared RGB combination at peak of macrophyte growth: a) Lac de Grand-Lieu (France); b) Fundu Mare Island (Romania); c) Mantua lakes system (Italy); d) detail area of Mantua lakes system with locations (see Table 1 for coordinates) of macrophyte samples collected *in situ* during 2015 (NIR band shown in greyscale).

3. Dataset

3.1.In situ data over Mantua lakes system

In situ sampling campaigns were performed by boat during the vegetative period 2015 (12 May, 11June, 16 and 31 July, and 9 September) in Mantua lakes system, collecting samples of *N. lutea* (NL), *T. natans* (TN), and *N. nucifera* (NN) over a total of 45 plots (three species sampled in three sites, with replicates, in five dates). In each sampling location, plot represents an area (~10 x 10 m) homogeneously covered by a species.

For each macrophyte plot, *in situ* georeferenced (Trimble GeoXM) photos (RGB camera Sony DSC-HX60; three photos each plot) were took from nadir, around 1 m above the canopy, framing a 1 m x 1 m square plot. Macrophyte LAI (m^2 m^{-2}) was derived by manually digitation of the areal size of each leaf (considering the overlapping of leaves) falling within the framed square plot of each image. As reported in detail in Villa et al. (2017), this method is more accurate for floating and floating-leaved species than for emerging leaves species, but the LAI underestimation for this latter species is not considered limiting for the aims of this work.

Spectral response data of different targets, including green grass, dry grass, bright and dark gravel, macrophyte canopy and water, were acquired *in situ* using high-resolution spectroradiometers (Spectral Evolution SR3500 and ASD FieldSpec Pro FR) during the campaigns of 12 May (9 plots), 11 June (6 plots), and 31 July 2015 (6 plots).

For each plot, measurements (five replicates) were acquired from adaxial surfaces at nadir (height above the plot ~50-100 cm; instrument field of view of 25°, corresponding to an area of 25-50 cm diameter). The reflectance spectra is calculated as the ratio between the acquired sample radiance and that recorded for a white reflectance standard (Spectralon white panel with near Lambertian properties). From replicates, the mean reflectance spectra for each surface target plot was

calculated, excluding spectral measurements with excessive environmental noise (values > ±2 standard deviation from the mean), due to background disturbance or atmospheric variation.

Table 1. Summary of the *in situ* dataset (*N. lutea* = *Nuphar lutea*; *N. nucifera* = *Nelumbo nucifera*; *T. natans* = *Trapa natans*).

Date	Sample ID	Species	Functional group	Lat (°N)	Lon (°E)	LAI (m^2 m^{-2})	Model cal.	Model val.
12 May 2015	NL1_132	*N. lutea*	Floating-leaved	45.1608	10.7344	0.89	x	
12 May 2015	NL2_132	*N. lutea*	Floating-leaved	45.1607	10.7346	0.70		x
12 May 2015	NL3_132	*N. lutea*	Floating-leaved	45.1608	10.7347	0.90	x	
12 May 2015	NN1_132	*N. nucifera*	Emergent	45.1571	10.7468	0.34	x	
12 May 2015	NN2_132	*N. nucifera*	Emergent	45.1587	10.7473	0.31		x
12 May 2015	NN3_132	*N. nucifera*	Emergent	45.1595	10.7432	0.37	x	
12 May 2015	TN1_132	*T. natans*	Floating	45.1611	10.7358	0.17	x	
12 May 2015	TN2_132	*T. natans*	Floating	45.1611	10.7354	0.45		x
12 May 2015	TN3_132	*T. natans*	Floating	45.1610	10.7352	0.19	x	
11 Jun 2015	NL1_162	*N. lutea*	Floating-leaved	45.1607	10.7348	0.93	x	
11 Jun 2015	NL2_162	*N. lutea*	Floating-leaved	45.1608	10.7346	0.95		x
11 Jun 2015	NL3_162	*N. lutea*	Floating-leaved	45.1608	10.7344	0.84	x	
11 Jun 2015	NN1_162	*N. nucifera*	Emergent	45.1593	10.7400	1.41	x	
11 Jun 2015	NN2_162	*N. nucifera*	Emergent	45.1570	10.7467	1.87		x
11 Jun 2015	NN3_162	*N. nucifera*	Emergent	45.1591	10.7470	1.48	x	
11 Jun 2015	TN1_162	*T. natans*	Floating	45.1608	10.7361	0.55	x	
11 Jun 2015	TN2_162	*T. natans*	Floating	45.1610	10.7355	0.77		x
11 Jun 2015	TN3_162	*T. natans*	Floating	45.1609	10.7351	0.84	x	
16 Jul 2015	NL1_197	*N. lutea*	Floating-leaved	45.1607	10.7344	1.18	x	
16 Jul 2015	NL2_197	*N. lutea*	Floating-leaved	45.1608	10.7342	1.12		x
16 Jul 2015	NL3_197	*N. lutea*	Floating-leaved	45.1608	10.7343	1.14	x	
16 Jul 2015	NN1_197	*N. nucifera*	Emergent	45.1593	10.7399	1.68	x	
16 Jul 2015	NN2_197	*N. nucifera*	Emergent	45.1570	10.7472	1.70		x
16 Jul 2015	NN3_197	*N. nucifera*	Emergent	45.1590	10.7475	1.49	x	
16 Jul 2015	TN1_197	*T. natans*	Floating	45.1608	10.7359	0.98	x	
16 Jul 2015	TN2_197	*T. natans*	Floating	45.1607	10.7354	1.02		x
16 Jul 2015	TN3_197	*T. natans*	Floating	45.1608	10.7351	0.95	x	
31 Jul 2015	NL1_212	*N. lutea*	Floating-leaved	45.1609	10.7342	1.11	x	
31 Jul 2015	NL2_212	*N. lutea*	Floating-leaved	45.1609	10.7342	1.11		x
31 Jul 2015	NL3_212	*N. lutea*	Floating-leaved	45.1609	10.7342	1.05	x	
31 Jul 2015	NN1_212	*N. nucifera*	Emergent	45.1594	10.7399	1.47	x	
31 Jul 2015	NN2_212	*N. nucifera*	Emergent	45.1572	10.7472	1.56		x
31 Jul 2015	NN3_212	*N. nucifera*	Emergent	45.1590	10.7475	1.62	x	
31 Jul 2015	TN1_212	*T. natans*	Floating	45.1608	10.7360	1.09	x	
31 Jul 2015	TN2_212	*T. natans*	Floating	45.1608	10.7356	1.00		x
31 Jul 2015	TN3_212	*T. natans*	Floating	45.1607	10.7351	0.98	x	
09 Sep 2015	NL1_252	*N. lutea*	Floating-leaved	45.1608	10.7348	0.96	x	
09 Sep 2015	NL2_252	*N. lutea*	Floating-leaved	45.1608	10.7346	1.11		x
09 Sep 2015	NL3_252	*N. lutea*	Floating-leaved	45.1608	10.7344	1.08	x	
09 Sep 2015	NN1_252	*N. nucifera*	Emergent	45.1590	10.7400	1.55	x	
09 Sep 2015	NN2_252	*N. nucifera*	Emergent	45.1571	10.7473	1.73		x
09 Sep 2015	NN3_252	*N. nucifera*	Emergent	45.1590	10.7474	1.51	x	
09 Sep 2015	TN1_252	*T. natans*	Floating	45.1607	10.7362	0.97	x	
09 Sep 2015	TN2_252	*T. natans*	Floating	45.1607	10.7356	1.04		x
09 Sep 2015	TN3_252	*T. natans*	Floating	45.1608	10.7350	1.02	x	

3.2.Satellite data

Medium resolution satellite data (10-30 m ground pixel), were collected over the three areas, following the macrophyte seasonality of year 2015. The bulk of these dataset is composed by scenes acquired during the SPOT5 (Take5) experiment, during which SPOT5 data were collected over 150 sites every 5 days under fixed geometry from April to September 2015. SPOT5 (Take5) aimed to simulate the acquisition of time series that ESA's Sentinel-2 full constellation will provide when both its satellite will be operational, around the beginning of 2018 (spot-take5.org). In order to complete the time series for covering the whole 2015, we used Landsat 7 ETM+ and Landsat 8 OLI scenes acquired earlier than April 2015, and Sentinel-2A MSI scenes acquired after September 2015. The whole dataset (Table 1) is composed of 45 scenes over the Mantua lakes system, 28 scenes over the Lac de Grand-Lieu, and 30 scenes over the Fundu Mare Island.

Table 2. Satellite data characteristics.

	DOY* of satellite scene acquisition in 2015 ***(WRS-2 path-row for Landsat; Relative Orbit number for Sentinel-2A)***		
	Mantua lakes system	Lac de Grand-Lieu	Fundu Mare Island
Landsat 7 ETM+		052(1), 068(1) **(201-027)**	
Landsat 8 OLI	093, 157°, 205°, 221° **(192-029)**	313**, 076 **(201-027)**	365**, 080(1) **(181-029)**
	004, 100°, 132°, 244° **(193-029)**		071(1) **(182-029)**
SPOT5 HRG	102, 112, 122(2), 127, 132, 137, 147(2), 157, 162, 167(2), 172(2), 177, 182, 187, 192, 197, 202, 207, 212(3), 217, 222(2), 227, 232, 242, 247, 252(4), 257°	99, 104, 109(3), 119, 129(2), 134(3), 139(2), 144(2), 159, 169(1), 174, 179, 184(3), 199(2), 204(1), 219(1), 224(1), 229(1), 244(2), 249(2)	100, 105, 110(4), 115(1), 125(1), 135, 140, 145, 155, 160(4), 165, 170(1), 175, 180, 190, 200, 205, 210(2), 220, 225(4), 240, 245, 250
Sentinel-2A MSI	185°, 205°, 225°, 245°, 255, 295 **(022)**	253, 273, 343 **(137)**	277, 317 **(050)**
	218°, 268, 328, 013*** **(065)**		364 **(007)**

*DOY: day of year (Julian day); **2014; ***2016; °used only for time series consistency check; cloud cover over the study area: 5-25%(1) 25-50%(2) 50-75%(3) 75-95%(4)

3.3.Ancillary data

In Lac de Grand-Lieu, the monitoring of the floating-leaved plants is carried out every three years with a specific series of aerial photos covering the central part of the lake. In 2015, this survey has been conducted on 8 August at 0.12 m resolution with good weather conditions. In order to compare the results with those of previous operations in the area, and due to limited computing capacity, the orthorectified pictures were reduced at 0.5 m resolution and processed to fit the range of the main floating macrophytes beds as well as that of an emergent macrophyte (*S. lacustris*). *N. lutea* and *N. alba* are not told apart, unlike beds of *T. natans* and beds of *N. peltata*. The surface covered by these four vegetation communities were calculated with a GIS (Quantum GIS Geographic Information System).

Fundu Mare Island was visited on 8 May, 8 June and 21 December 2015, and a field survey was carried out between 9 and 16 July 2015 in order to improve the understanding of the hydrological processes at the island. Between 9 June and 21 December 2015, the water level at FM was recorded at three sites in the lakes using pressure sensors (Global Water). The water level upstream from the weir in the main outlet channel (Hogioaia channel) was measured at four dates and its temporal development between these dates was estimated based on the water balance (Zinke et al. 2016). Figure 2 shows the water levels in 2015, with reference to the geodetic datum Black Sea Sulina (MNS), and the typical macrophyte arrangement with site hydrology characteristics.

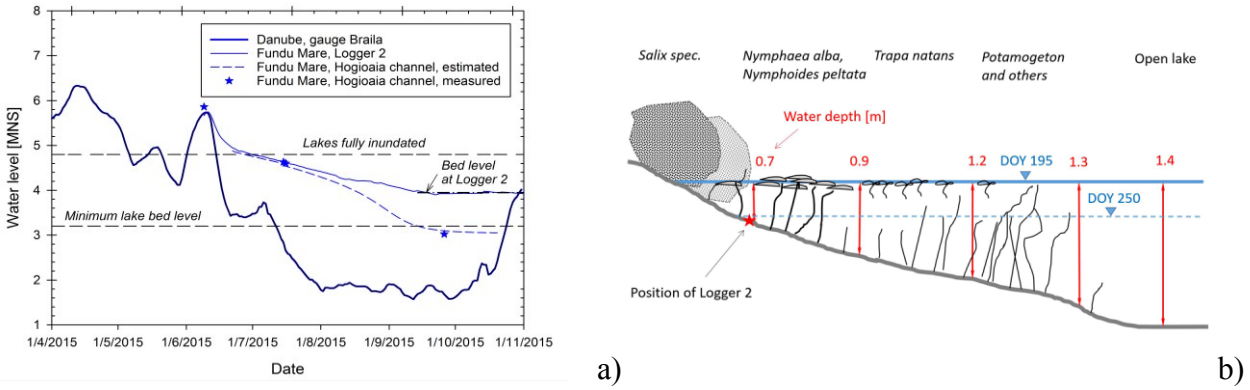

a) b)

Figure 2. Relations between macrophyte and hydrology in Fundu Mare Island: a) water levels of the Danube (gauge Braila), in Lake Misaila (Logger 2) and upstream from the weir in the Hogioaia channel. Note that the lake water level dropped below the bed elevation at the logger site (3.95 MNS); b) sketch of typical water depths that were measured for different macrophyte community types during the field survey on 14 July 2015 (DOY 195), at lake stage 4.65 MNS. The figure includes the elevation position for Logger 2 in Lake Misaila and the measured lake water level on 7 September 2015 (DOY 250).

The status of the vegetation during the field activities in June and July was documented by georeferenced photos that were spot-wise taken with a digital camera (Olympus, with GPS positioning of images). In combination with some notes taken during the field survey, these photos allowed identifying the dominating macrophyte community types and species, as illustrated in Figure 2b.

On 13 and 14 July 2015, water depths ranging between 0.7 and 1.5 m were measured in the densely vegetated lakes from the boat using a folding rule at selected locations. This information was correlated with the observed vegetation type and allowed for a rough estimation of the water depths belonging to a given vegetation type for the date of the observation (Figure 2b).

The overall status of the vegetation in September 2015 was documented during a remote sensing survey using a professional survey-grade mapping Unmanned Aerial Vehicle (UAV; Parrot SenseFly eBee), mounted with a high resolution 16.1 Mpixels digital camera (Canon IXUS 127 HS). During the survey, almost eight thousand photos were taken from around 200 m flight height, covering an area larger than 2000 ha (half land, half water), with nominal pixel size on the

ground varying between 2 and 5 cm. These data were used to generate an orthomosaic of the whole area.

4. Methods

4.1.Satellite data pre-processing

SPOT5 data were retrieved from the ESA-CNES webportal (https://spot-take5.org), for the three sites that contain our study areas, namely: 'Italia: Mantua' (Mantua lakes system), 'France: Pornic' (Lac de Grand-Lieu), and 'Romania: Braila' (Fundu Mare Island). SPOT5 data were retrieved as Level 2A products, which are ortho-rectified surface reflectance, corrected from atmospheric effects (including adjacency), using the Multi-sensor Atmospheric Correction and Cloud Screening processor (MACCS; Hagolle et al., 2015).

Landsat scenes were pan-sharpened at 15 m resolution, using the Gram-Schmidt method (Laben and Brower, 2000). For Landsat 7 data, SLC-off gaps were filled using the approach developed by Maxwell et al. (2007).

Landsat and Sentinel-2A data were radiometrically calibrated and converted to surface reflectance using ATCOR-2 code (Richter and Schläpfer, 2014). ATCOR-2 was run using image-based visibility estimation (Kaufman et al., 1997) and adjacency effect compensation (1 km radius).

Homologous spectral bands from the multi-sensor dataset were retained for further processing, by selecting the better matching with four broadband spectral ranges:

- Green surface reflectance: ETM+ band 2, OLI band 3, HRG band 1, MSI band 3;
- Red surface reflectance: ETM+ band 3, OLI band 4, HRG band 2, MSI band 4;
- NIR surface reflectance: ETM+ band 4, OLI band 5, HRG band 3, MSI band 8;

- SWIR1 surface reflectance: ETM+ band 5, OLI band 7, HRG band 4, MSI band 11.

To ensure geometric consistency of the multi-sensor dataset, pre-April Landsat scenes were co-registered with earliest available cloud free SPOT5 scene (12 April for Mantua lakes system, 9 April for Lac de Grand-Lieu, 10 April for Fund Mare island), and post-September Sentinel-2A scenes were co-registered with latest available cloud free SPOT5 scene (04 September for Mantua lakes system, 17 August for Lac de Grand-Lieu, 7 September for Fund Mare Island). 20 tie points on each pair of images were collected and co-registration was carried out through affine transformation (6 parameters). Root Mean Square Error (RMSE) and maximum planimetric error were calculated for the tie points of each coregistered scene pair.

Relative radiometric consistency of the multi-sensor dataset was checked for the Mantua lakes system data by comparing surface reflectance of 15 artificial surface targets used as pseudo-invariant features (PIFs) and 5 macrophyte beds of different species, extracted from matchup pairs of SPOT5-Landsat 8 scenes (6 pairs) and of SPOT5-Sentinel-2A scenes (5 pairs), with maximum acquisition date difference of ±2 days. The linear coefficient of determination (R^2), and Mean Absolute Error (MAE) of surface reflectance values extracted from each scene pair were calculated and pooled by sensor coupling.

Absolute radiometric accuracy of Landsat 8 and SPOT5 data acquired over Mantua lakes system was assessed against *in situ* spectra collected simultaneously (maximum ±1 hour difference) to satellite acquisitions (12 May for Landsat 8, 12 May, 11 June and 16 July for SPOT5) during fieldwork. *In situ* spectra were acquired over 21 targets, both terrestrial and aquatic: dry and green grass, gravel, macrophytes and water. The R^2, and MAE between *in situ* and satellite-derived reflectance were calculated for each spectral band and then grouped by sensor, to give a synthetic measure of radiometric accuracy.

4.2.Modelling macrophyte LAI

Following the approach of Villa et al. (2017), macrophyte LAI maps were derived from satellite data through semi-empirical regression modelling based on spectral indices (SIs). Macrophyte LAI data collected *in situ* during 2015 growing season in Mantua lakes system were split into two subsets: two-thirds were used for calibrating (30 samples), and one third for validation (15 samples) of the semi-empirical LAI model implemented.

A range of ten SIs sensitive to vegetation canopy morphology and based on broadband surface reflectance in the four ranges cited above (Green, Red, NIR, and SWIR1), matching SPOT5 HRG bands - were tested (Table 2, including related references). The 4 band broadband reflectance spectra of each macrophyte plot sampled in Mantua lakes system were derived from SPOT5 HRG Level 2A acquired within 5 days from *in situ* data collection. SPOT5 HRG spectra were extracted from 3 x 3 m pixel windows centred on the location of *in situ* samples, retaining the maximum vegetated pixel as matchup (Villa et al., 2017).

All matchup spectra (N=45) were then used to derive the SIs listed in Table 2, for both calibration and validation sample sets. The coefficient of determination (R^2) between *in situ* macrophyte LAI and the SPOT5 HRG derived SIs for the calibration set (N = 30) was used as indicator of goodness of fit to inform the selection of the best SI for LAI modelling through linear regression (see last column of Table 2).

LAI model performance was assessed in terms of Mean Absolute Error (MAE), Mean Absolute Percentage Error (MAPE), and R^2, calculated over the separate validation set (N = 15).

Table 3. Spectral Indices tested.

Name	Acronym	Formula	Reference	R^2 *vs.* LAI
Enhanced Vegetation Index 2	EVI2	$2.4\frac{\rho_{NIR}-\rho_{Red}}{\rho_{NIR}+\rho_{Red}+1}$	Jiang et al., 2008	0.889
Modified Triangular Vegetation Index 1	MTVI1	$1.2[1.2(\rho_{NIR}-\rho_{Green})-2.5(\rho_{Red}-\rho_{Green})]$	Haboudane et al., 2004	0.884
Soil Adjusted Vegetation Index	SAVI	$1.5\frac{\rho_{NIR}-\rho_{Red}}{\rho_{NIR}+\rho_{Red}+0.5}$	Huete, 1988	0.884
Triangular Vegetation Index	TVI	$0.5[120(\rho_{NIR}-\rho_{Green})-200(\rho_{Red}-\rho_{Green})]$	Broge and Leblanc, 2001	0.884
Aerosol free vegetation index	AFRI	$\rho_{NIR}-0.66\frac{\rho_{SWIR1}}{\rho_{NIR}+0.66\rho_{SWIR1}}$	Karnieli et al., 2001	0.883
Modified Chlorophyll Absorption in Reflectance Index 2	MCARI2	$1.5\frac{2.5(\rho_{NIR}-\rho_{Red})-1.3(\rho_{NIR}-\rho_{Green})}{\sqrt{(2\rho_{NIR}+1)^2-(6\rho_{NIR}-5\sqrt{\rho_{Red}})-0.5}}$	Haboudane et al., 2004	0.880
Green Soil Adjusted Vegetation Index	GSAVI	$1.5\frac{\rho_{NIR}-\rho_{Green}}{\rho_{NIR}+\rho_{Green}+0.5}$	Tian et al., 2005	0.876
Normalized Difference Vegetation Index	NDVI	$\frac{\rho_{NIR}-\rho_{Red}}{\rho_{NIR}+\rho_{Red}}$	Rouse et al., 1974	0.807
Green Normalized Difference Vegetation Index	GNDVI	$\frac{\rho_{NIR}-\rho_{Green}}{\rho_{NIR}+\rho_{Green}}$	Gitelson and Merzlyak, 1994	0.774
Specific Leaf Area Vegetation Index	SLAVI	$\frac{\rho_{NIR}}{\rho_{Red}+\rho_{SWIR1}}$	Lymburner et al., 2000	0.605

The macrophyte LAI model implemented was then applied to the satellite dataset comprising our three study areas (Table 1). LAI maps were produced only for the areas covered by floating and emergent macrophytes, which were isolated by using a binary raster mask (mask value = -1) composed by all pixels belonging to the water body area delineated using pre-season data (i.e. with maximum EVI2 < 0.05 in January-April), and covered by vegetation during the growing season (i.e. with maximum EVI2 > 0.1 in April-September).

4.3.Macrophyte LAI time series

For every scene, cloud covered areas, identified as pixels with ρ_{Green} > 0.15 surrounded by 50 m buffer, were masked out from macrophyte LAI maps (mask value = -1). Subsequently, and in order to homogenise spatial resolution of products derived from multiple sensors with different

original resolution (Landsat, SPOT5 and Sentinel-2A), macrophyte LAI maps were all resampled at 20 m pixel size.

Time series of macrophyte LAI for the whole 2015 year with 5 day temporal resolution - thus matching the revisit of SPOT5 Take5 dataset (as well as that of Sentinel-2A/2B joint constellation operational in the future) - were established by filling missing dates (5 day time steps) in the periods not covered by SPOT5 Take 5 acquisitions (pre-April with Landsat, post-September with Sentinel-2A, see Table 1), with void layers (NA value = -1).

4.4.Metrics of seasonal dynamics

Quantitative descriptors of macrophyte seasonal dynamics were derived using TIMESAT software with macrophyte LAI maps produced as input (Jönsson and Eklundh, 2002; Jönsson and Eklundh, 2004). TIMESAT output parameters considered, hereafter called seasonal dynamics metrics, were (Figure 3): the time of the start of the season (SoS, in Day of Year: DOY), time for the peak of the season (PoS, in DOY), the time of the end of the season (EoS, in DOY), the length of season (S_length, in days), the maximum LAI value reached during the season (LAI_max, in m^2_{veg} m^{-2}), the rate of increase of LAI during the early vegetative phase (LAI_growth, in m^2_{veg} m^{-2} d^{-1}), the rate of decrease of LAI during the senescence phase (LAI_senescence, in m^2_{veg} m^{-2} d^{-1}), the seasonal integral between the fitted LAI curve and the baseline value from SoS to EoS (LAI_productivity, in m^2_{veg} m^{-2} d).

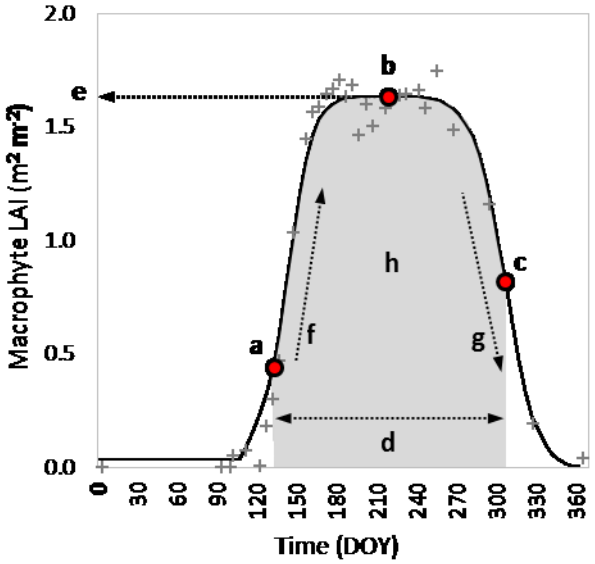

Figure 3. Metrics of seasonal dynamics derived from macrophyte LAI time series using TIMESAT: (a) SoS, (b) PoS, (c) EoS, (d) S_length, (e) LAI_max, (f) LAI_growth, (g) LAI_senescence, (h) LAI_productivity. Grey crosses are single date punctual values, and black line is the fitted asymmetric Gaussian curve. Adapted from Eklundh and Jönsson (2015).

TIMESAT was run without applying any spike filtering and setting the envelope iterations number to one. The curve fitting method selected was based on Asymmetric Gaussian curves, because it was demonstrated to be less sensitive to noise and incompleteness of input time series (Gao et al., 2008; Tan et al., 2011). According to our observations of macrophyte species investigated, the start of season occurs when macrophytes overpass 25% of peak LAI (i.e. 0.25 of the fitted curve amplitude, before PoS), and the end of season is flagged when macrophyte LAI decrease during senescence phase under 50% of reached maximum (i.e. 0.50 of the fitted curve amplitude, after PoS). For further details on TIMESAT requirements, capabilities and outputs the reader is referred to the software manual (Eklundh and Jönsson, 2015).

4.5.Influence of input variables on macrophyte phenology estimation

We evaluated the influence of some characteristics of the time series input dataset on the

macrophyte seasonal dynamics results by assessing the variability of key seasonality metrics derived as TIMESAT outputs, namely the SoS, PoS, and EoS, when the input multi-temporal dataset is changed. In particular, we investigated the sensitivity of SoS, PoS, and EoS to i) could cover amount in input time series; ii) temporal resolution of input time series; and iii) relative importance of single dates or periods across the macrophyte growing season (April-September). We carried out this analysis using the Mantua lakes system dataset, which is the most complete and for which we collected field measures and observations during 2015 macrophyte growing season. We compared the SoS, PoS, and EoS derived from the baseline macrophyte LAI time series input, with maximum theoretical time revisit of 5 days during the SPOT5 Take5 experiment (hereafter named Mantua_5d, see Table 1), with the same seasonal metrics calculated when input to TIMESAT was varied as described in the following. The comparison was carried out by calculating differences in SoS, PoS, and EoS outputs over four selected macrophyte beds with different dominating species, environmental conditions and seasonality features (see Figure 4). For this purpose, we calculated MAE, and minimum to maximum span (Max_span) differences between SoS, PoS, and EoS derived from modified and baseline input dataset.

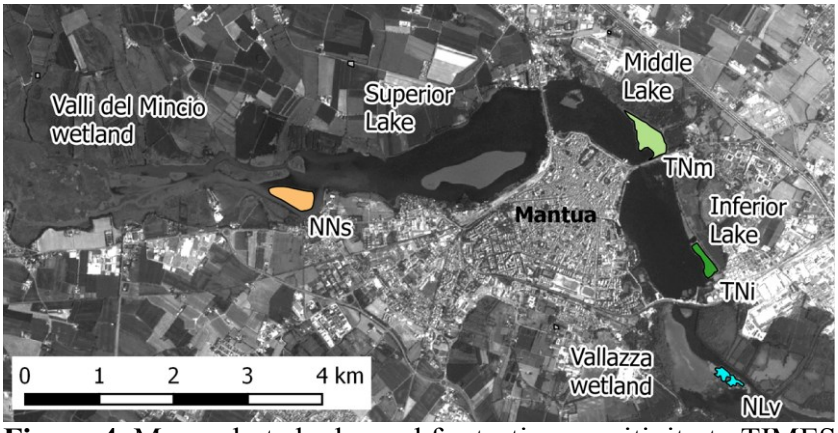

Figure 4. Macrophyte beds used for testing sensitivity to TIMESAT outputs over Mantua lakes system area. NNs = *Nelumbo nucifera* bed (Superior Lake); TNm = *Trapa natans* bed (Middle Lake); TNi = *Trapa natans* bed (Inferior Lake); NLv = *Nuphar lutea* bed (Vallazza wetland).

4.5.1. Influence of could cover amount

For assessing the influence of cloud cover amount, three modified input dataset were prepared, by setting different thresholds on cloud cover amount for each scene (see Table 1): maximum cloud cover allowed of 50% (2 scenes removed, Mantua_5d_CC50); maximum cloud cover allowed of 30% (4 scenes removed, Mantua_5d_CC30); maximum cloud cover allowed of 10% (7 scenes removed, Mantua_5d_CC10).

4.5.2. Influence of temporal resolution

For assessing the influence of temporal resolution, five modified input dataset were prepared at 10-day, aimed to simulate Sentinel-2A revisit, and 15-day revisit, aimed to simulate Landsat series revisit (16 days). Two dataset with 10-day temporal resolution were produced by removing one every two dates in the baseline dataset, starting from DOY 2 (Mantua_10d_a), or from DOY 7 (Mantua_10d_b). Three dataset with 15-day temporal resolution were produced by removing two every three dates in the baseline dataset, starting from DOY 2 (Mantua_15d_a), from DOY 7 (Mantua_15d_b), or from DOY 12 (Mantua_15d_c).

4.5.3. Influence of missing acquisitions

For simulating the influence of missing dates during the macrophyte growing season (April - September in temperate areas), possibly occurring because of cloud cover, extreme atmospheric conditions, or other issues due to the sensor (e.g. maintenance or failed acquisitions), 46 modified input dataset were prepared at 5-day and 15-day revisit. 31 dataset with nominal 5-day temporal resolution were prepared, each produced by removing one single date in the original SPOT5 Take5 dataset (Mantua_5d_1-31, depending on which date is removed). 15 dataset with nominal 15-day temporal resolution were prepared, each produced by removing one single date acquired from April to early September in the resampled Mantua_15d_b dataset (Mantua_15d_b_1-15,

depending on which date is removed).

5. Results

5.1. Time series consistency

Multitemporal registration of Landsat and Sentinel-2A scenes coregistered with SPOT5 scenes is adequate to common requirements for the geometric consistency of gridded time series data (Dai and Khorram, 1998), i.e. with respect to the tie points used, planimetric RMSE is lower than 0.2 pixels (4 m) and maximum planimetric error is lower than 0.3 pixels (6 m).

Surface reflectance of homologous SPOT5 HRG and Landsat 8 OLI bands, calculated over the 6 matchup pairs acquired with less than 2 days difference (1.2 days in average) over Mantua lakes system displayed good consistency, with MAE in the range 0.028-0.041 (14-23% in relative terms) and $R^2 > 0.86$. For the 5 SPOT5 HRG – Sentinel-2A MSI matchup pairs acquired with less than 2 days difference (1.8 days in average), similar but slightly higher differences were scored, with MAE in the range 0.033-0.045 (14-31% in relative terms) and $R^2 > 0.71$.

Figure 5 shows the comparison between EVI2 scores derived from SPOT5 data and Landsat 8 (Figure 5a) or Sentinel-2A (Figure 5b) matchup pairs. Consistency between these sets are still good, but with errors up to 55% in relative terms and a tendency towards underestimation of low EVI2 scores as well as to overestimation of high EVI2 values for both Landsat 8 and Sentinel-2A (regression slope higher than 1.3), when compared to SPOT5 dataset.

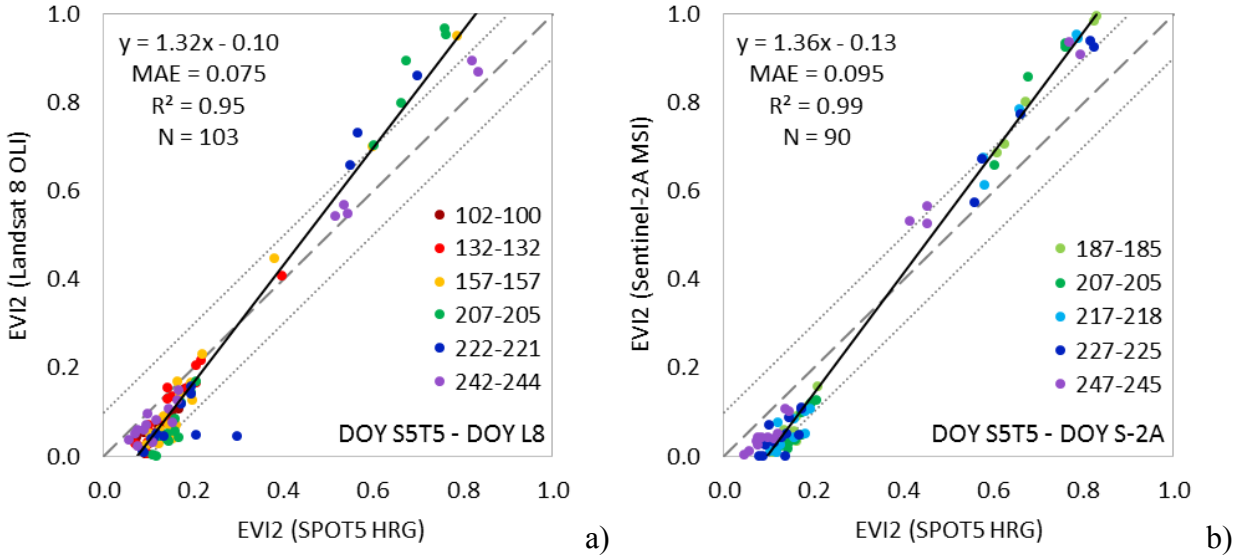

Figure 5. Comparison of EVI2 calculated from SPOT5 HRG surface reflectance data with EVI2 calculated from satellite scenes acquired in different dates (within 2 days maximum) with: a) Landsat 8 OLI; b) Sentinel-2A MSI. Dashed line is the 1:1, dotted lines mark the ±0.1 error line. DOY = day of year (Julian day).

The radiometric accuracy of Landsat 8 OLI and SPOT5 HRG was carried out by comparing surface reflectance derived from atmospherically corrected scenes with *in situ* spectra acquired during the satellite overpass over Mantua lakes system (less than 1-hour difference). Spectral reflectance in the visible, i.e. in broadband green and red ranges, was more accurate with respect to *in situ* spectra, scoring MAE around 0.03-0.04 for both SPOT5 and Landsat 8 (Figure 6). Higher but still limited errors are scored in NIR and SWIR range spectral bands, with MAE around 0.06-0.07. Overall, both SPOT5 HRG and Landsat 8 OLI surface reflectance shows a tendency to overestimate *in situ* reflectance for low values and to underestimate it for higher values (*in situ* vs satellite reflectance slope = 0.73-0.74, intercept = 0.05).

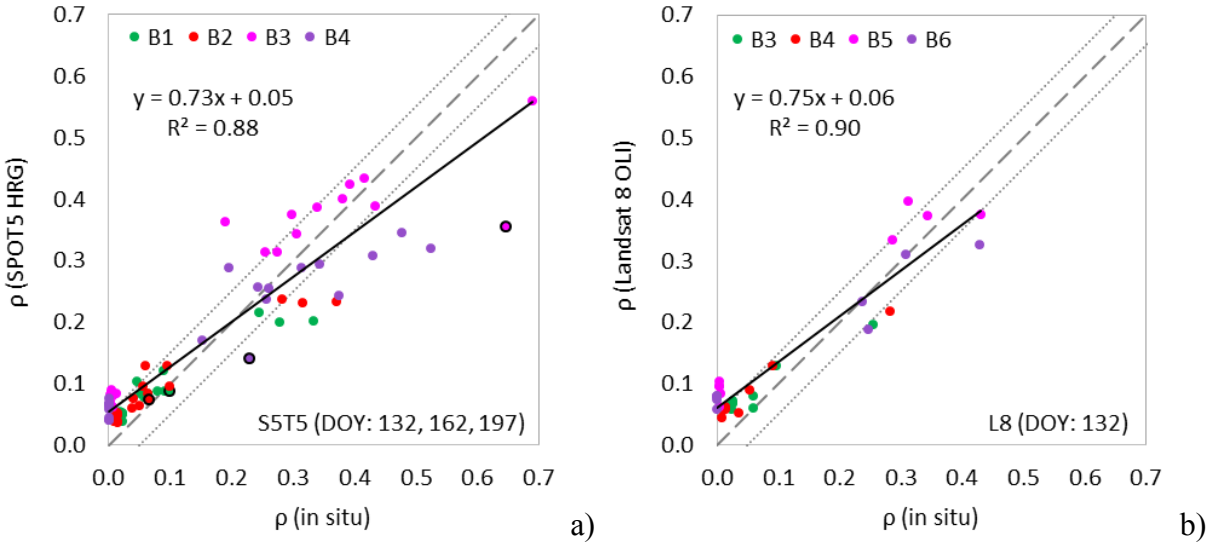

		ρ Green	ρ Red	ρ NIR	ρ SWIR1
		Band 1	Band 2	Band 3	Band 4
SPOT5 HRG	MAE	0.036	0.040	0.067	0.067
	R^2	0.92	0.93	0.94	0.91
		Band 3	Band 4	Band 5	Band 6
Landsat 8 OLI	MAE	0.037	0.042	0.072	0.060
	R^2	0.92	0.95	0.95	0.96

c)

Figure 6. Comparison of *in situ* spectra with surface reflectance (ρ) derived from satellite data collected simultaneously (maximum 1 hour difference) from: a) SPOT5 HRG spectral bands; b) Landsat 8 OLI spectral bands; c) accuracy metrics calculated. Dashed line is the 1:1, dotted lines mark the ±0.05 error line (B1 = band 1; B2 = band 2; B3 = Band 3; B4 = Band 4; B5 = Band 5; B6 = Band 6).

5.2.Modelling macrophyte LAI

EVI2, being the SI derived from SPOT5 HRG scoring highest R^2 with *in situ* macrophyte LAI for the calibration set (R^2 = 0.889, Table 2), was used for implementing the semi-empirical LAI model through linear regression using equation (1):

$$\text{LAI } (m^2\ m^{-2}) = 2.015(\text{EVI2}) + 0.048 \qquad \text{Range: } [0.0\text{–}2.0\ m^2\ m^{-2}] \qquad (1)$$

Comparison between LAI measured *in situ* and LAI model outputs (Figure 7) shows an overall error level of 0.11 $m^2\ m^{-2}$ in absolute terms (MAE), for both calibration and validation sample

sets, and lower than 20% in relative terms (MAPE of 17.7% and 9.6% for calibration and validation sets, respectively). Over both sample sets, the model tends to underestimate LAI values higher than 1.5-1.6 m^2 m^{-2} (corresponding to mature *N. nucifera* plots), with some mismatch at intermediate LAI values for *T. natans* (~20% overestimation of LAI > 1 m^2 m^{-2}) and *N. lutea* (15-25% underestimation of low LAI conditions).

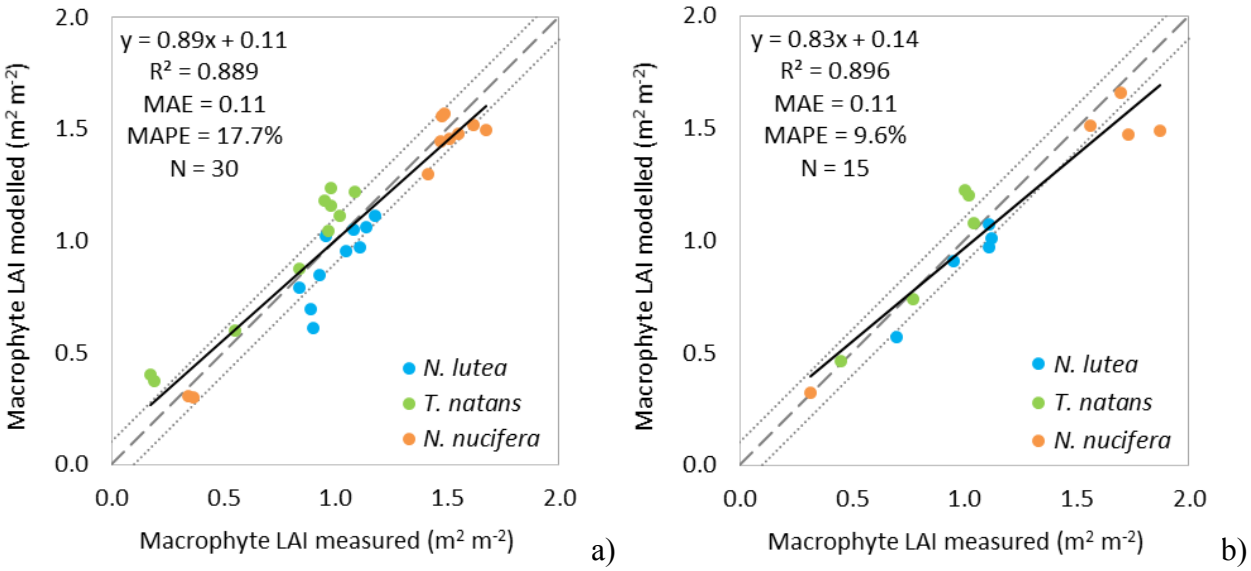

Figure 7. Comparison of macrophyte LAI measured in situ with estimates derived from the EVI2 based semi-empirical linear model implemented (SPOT5 HRG scenes), over: a) calibration set; b) validation set. Dashed line is the 1:1, dotted lines mark the ±0.1 error line (*N. lutea* = *Nuphar lutea*; *T. natans* = *Trapa natans*; *N. nucifera* = *Nelumbo nucifera*).

5.3.Mapping macrophyte seasonal dynamics

5.3.1. Mantua lakes system

Macrophyte seasonal dynamic maps derived for Mantua lakes system are reported in Figure 8. The time of the start of the season was quite different between the investigated lakes, in particular at Superior Lake *N. nucifera* started to grow in mid-May (DOY 125-135), whereas *T. natans* appeared in mid-May (DOY 130-140) and early June (DOY 155-165) at Inferior and Middle lakes, respectively (Figure 8a). The peak of season was quite homogeneous (from late July to

middle August) between species, except for *T. natans* at Inferior Lake where it was reached on mid-July (Figure 8b). In fact, for this latter stand the end of season was mid-late August, while the species disappeared at Middle Lake about one month later (Figure 8c). The last species that started the senescence period was *N. nucifera* (late October, Figure 8c).

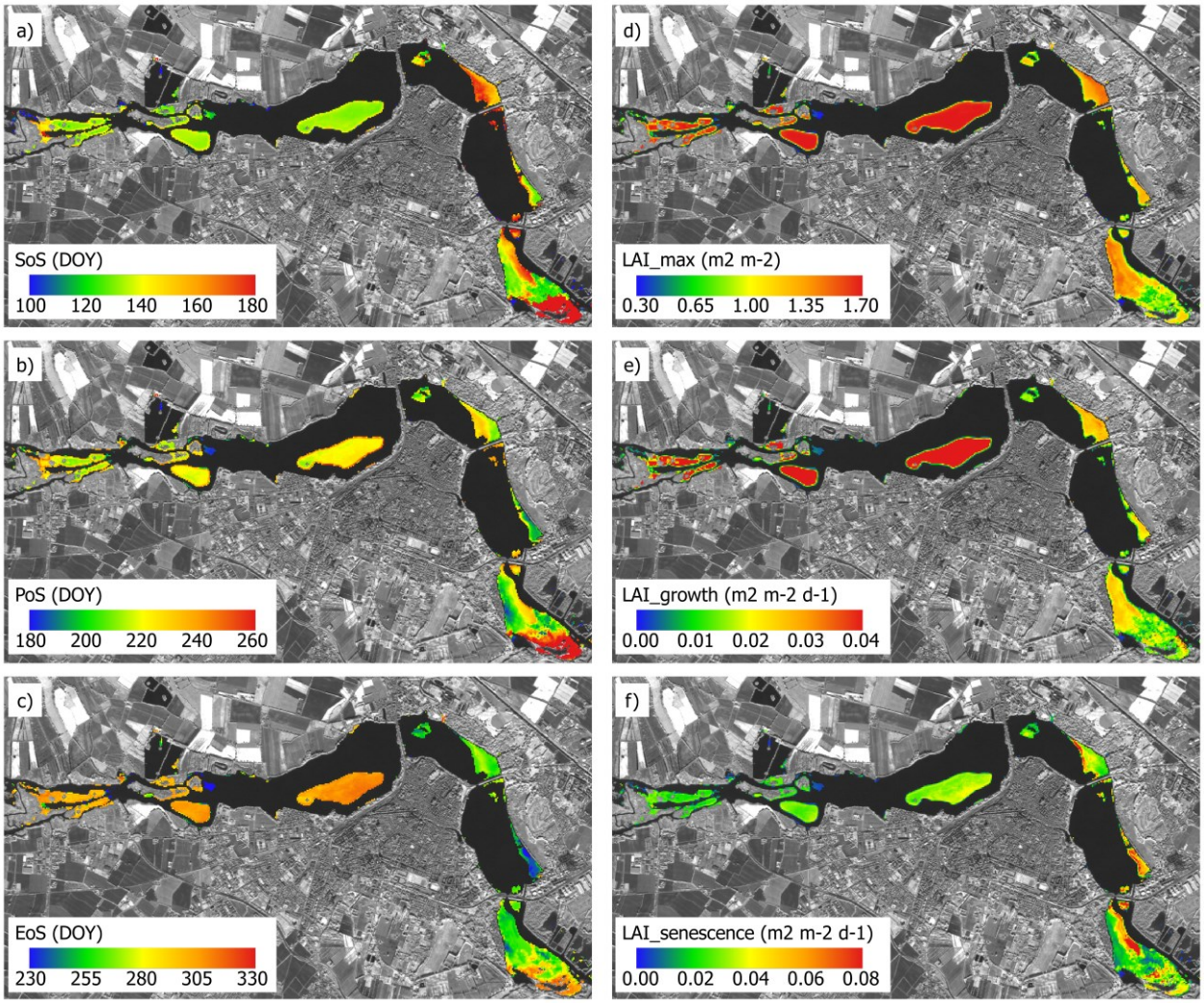

Figure 8. Macrophyte seasonal dynamics maps for Mantua lakes system study area: a) SoS; b) PoS; c) EoS; d) LAI_max; e) LAI_growth; f) LAI_senescence. SoS = start of season, PoS = peak of season, EoS = end of season, LAI_max = maximum LAI value, LAI_growth = rate of increase of LAI during the early growth, LAI_senescence = rate of decrease of LAI during the senescence.

N. nucifera LAI values were higher than *T. natans* ones during the early and maximum

vegetative phases, on the contrary, during the senescence phase the LAI decrease rates were more homogenous, especially at Middle Lake (Figures 8d, 8e, 8f). The length of season of *N. nucifera* and *T. natans* were up to 180 and 120 days, respectively. *T. natans* maximum LAI values at Middle Lake stand were higher than those at Inferior Lake (Figure 8d). In these two lakes the *T. natans* LAI values were similar during the early vegetative phase (Figure 8e), while during the senescence phase the LAI decrease rate was higher at Inferior Lake compared to Middle Lake one (Figure 8f). At Vallazza wetland, the macrophyte population was composed by different species, including *T. natans* and *N. lutea*, which reflects in more patched dynamics.

5.3.2. Lac de Grand-Lieu

The seasonal dynamics maps derived for Lac de Grand-Lieu show a precocious development of the nymphaeids in the south of the central part of the lake, growing in protected bays with higher water transparency. The fastest species to develop is *T. natans*, which is well highlighted by small blue spots in the middle of the lake in Figure 9b and 9c, showing anticipated PoS and EoS, around DOY 180 and 230, respectively. The peak value of LAI mapped for this species in 2015 (0.4-0.6) is lower than what observed in the field in previous years, when *T. natans* beds were more dense.

The early season development dynamics are shifted in time depending on the areas. The areas dominated by *N. lutea*, with a very low water level are in the south of the lake, show a precocious peak (DOY 180-185) and a high LAI growth rate. Additional analysis focusing on the balance between *N. alba* and *N. lutea* is needed in order to investigate the difference between these different places with the same date of PoS and a moderate high LAI growth but with a shifted vegetation peak. The areas with the latest EoS (DOY 295 to 330, Figure 9c) could be again attributed to dominance of *N. alba*, but the mix of this species with *N. lutea* in most of the parts

of the lake dos not allow conclusive remarks without further data and analysis.

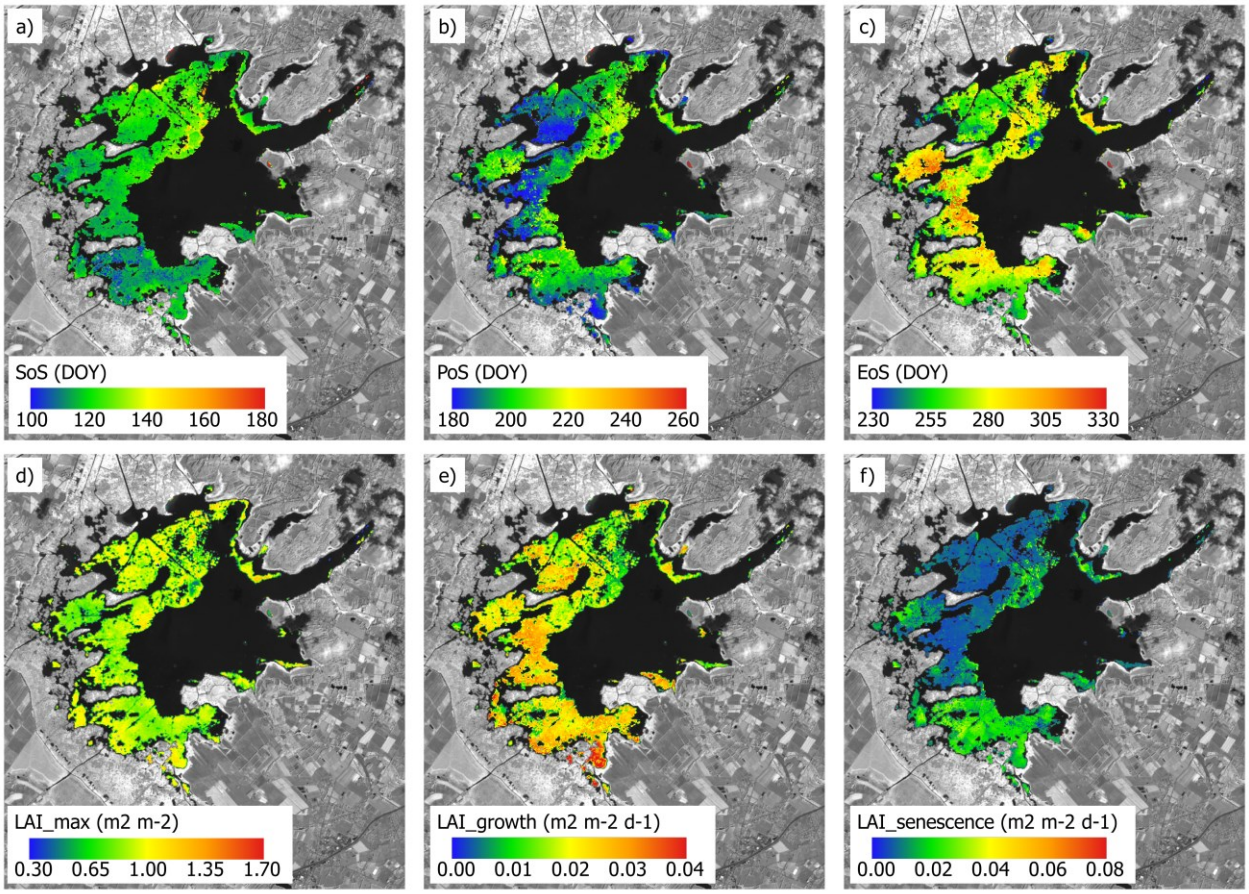

Figure 9. Macrophyte seasonal dynamics maps for Lac de Grand-Lieu test site: a) SoS; b) PoS; c) EoS; d) LAI_max; e) LAI_growth; f) LAI_senescence. Abbreviations are the same as in Figure 8.

5.3.3. Fundu Mare Island

The seasonal vegetation dynamics at Fundu Mare Island in 2015 reflects the changing hydrological conditions throughout the growing season. The coloured zones in Figure 10 mark the extent of the water covered area when the lakes are inundated completely (April-June, in 2015), before the lake water levels decreased in summer (Figure 2).

The maps of macrophyte seasonal dynamics of Fund Mare Island show that the SoS for most of the area, in particular the aquatic ecosystems, occurred between DOY 116 and 132, i.e. end of April and beginning of May. SoS as late as on DOY 180 (late June) was observed in zones with

massive willow encroachment. The PoS of floating plants ranges between 195 and 220 (mid to late July), and between 230 and 265 (August to September) for the zones that dried up when the water level dropped by around 2 m with respect to seasonal maximum (early August, Figure 2). The EoS values show again a clear difference between the deepest lake areas with DOY 250 to 270 and outer zones that were dry during the later season.

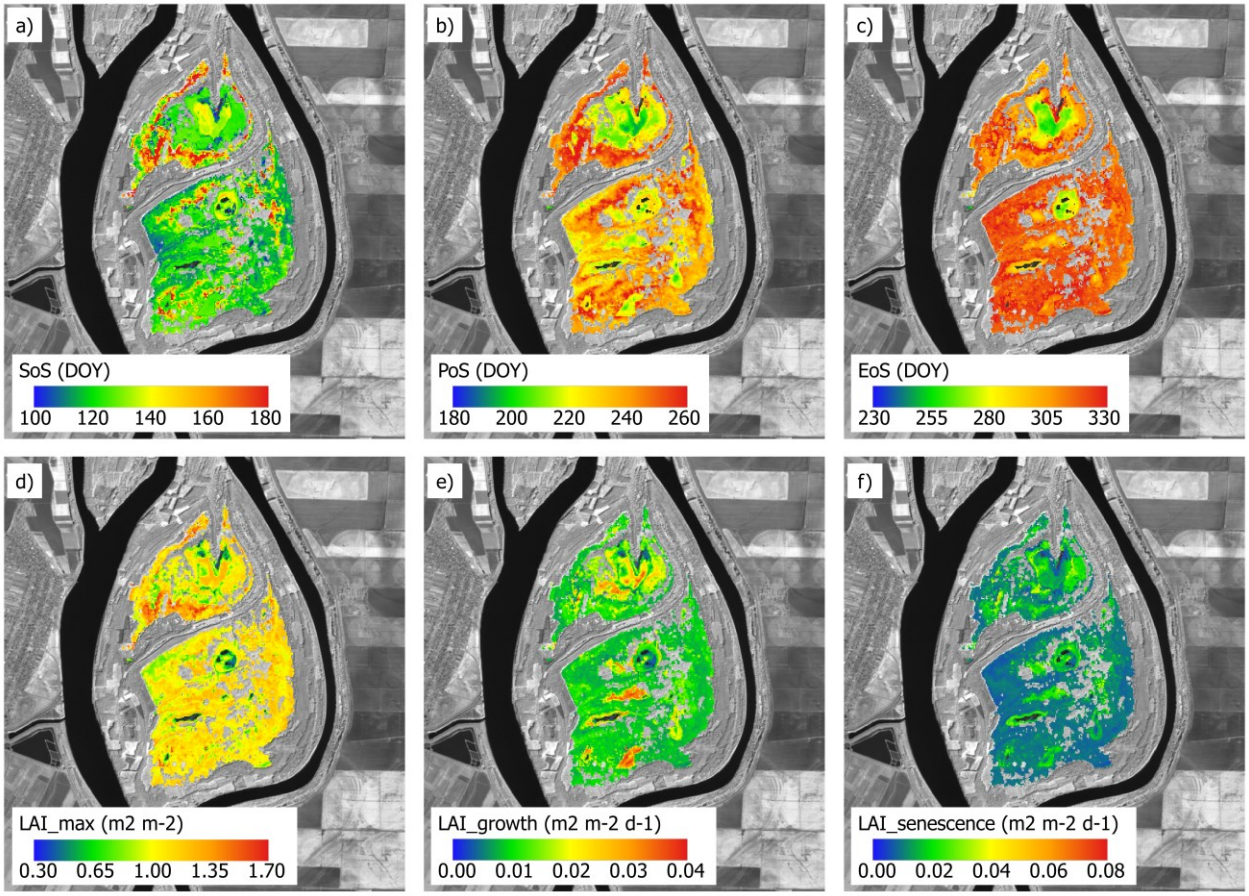

Figure 10. Macrophyte seasonal dynamics maps for Fundu Mare Island test site: a) SoS; b) PoS; c) EoS; d) LAI_max; e) LAI_growth; f) LAI_senescence. Abbreviations are the same as in Figure 8.

The differences between the vegetation communities and the respective inundation duration are also reflected in the peak LAI value and the rate of LAI change during growth and senescence. The highest peak LAI (1.35 to 1.65 m^2 m^{-2}) were mapped at the southwestern edge of Lake

Chiriloaia, where terrestrial species develop with low water level in late July. Small patches with LAI > 1.25 were found at many locations in both lakes and can be related to the willows-helophyte mosaic (see Figure 2b).

The highest rates of LAI change (Figures 10e and 10f) were observed for deeper lake areas, covered by floating and floating-leaved species, while the upland areas, inhabited by a mosaic of willows and helophytes, show a different and more gradual growth seasonality.

5.4. Influence of input variables on macrophyte phenology estimation

Table 4. Influence of cloud cover amount in input time series on TIMESAT output metrics (SoS, PoS, EoS) for Mantua lakes system dataset.

		Difference *vs*. baseline (Mantua_5d)		
		ΔSoS (days)	**ΔPoS (days)**	**ΔEoS (days)**
Mantua_5d_CC10	NNs	0.5	-0.1	-0.6
	TNm	0.7	-0.1	0.1
	TNi	-1.1	0.8	0.0
	NLv	-0.4	0.6	0.0
	MAE	**0.68**	**0.31**	**0.28**
	Max_span	*1.83*	*0.93*	*0.76*
Mantua_5d_CC30	NNs	-1.4	0.3	0.5
	TNm	0.0	0.0	0.1
	TNi	-0.6	0.0	-0.2
	NLv	-0.8	-0.4	0.0
	MAE	**0.76**	**0.19**	**0.27**
	Max_span	*1.44*	*0.75*	*0.70*
Mantua_5d_CC50	NNs	0.0	0.0	0.0
	TNm	0.0	0.0	0.0
	TNi	0.3	0.3	-0.2
	NLv	0.0	0.0	0.0
	MAE	**0.06**	**0.07**	**0.04**
	Max_span	*0.25*	*0.34*	*0.17*

Macrophyte test beds: NNs: *N. nucifera* (Superior Lake); TNm: *T. natans* (Middle Lake); TNi: *T. natans* (Inferior Lake); NLv: *N. lutea* (Vallazza wetland)

5.4.1. Influence of cloud cover amount

As shown in Table 4, under varying cloud cover threshold the difference in phenology timing metrics with respect to the baseline is under 1.5 days, across all macrophyte species investigated.

Averaged over all test sample beds, the MAE is lower than 0.8 days, and Max_span is under 1.9 days. Phenology timing outputs with maximum 50% cloud cover (Mantua_5d_CC50) shows only slight differences with respect to the baseline (Max_span < 0.3 days), while results using 30% and 10% maximum cloud cover are a little more diverging, scoring Max_span of 1.5 and 1.9 days, respectively. Among timing metrics tested, SoS is more sensitive to changes in cloud cover threshold choice (MAE < 1.9 days), compared to PoS and EoS (MAE < 0.9 days).

5.4.1. Influence of temporal resolution

Table 5 summarizes the differences in timing metrics with respect to baseline when the time revisit of the input time series is reduced to 10 or 15 days.

When the temporal resolution is degraded to 10 days, as for nominal Sentinel-2A coverage over Europe and Africa and for Sentinel-2A and -2B constellation globally, differences in SoS, PoS and EoS across all macrophyte species test beds do not exceed 3.9 days. Different test beds, representing different macrophyte communities, show variable sensitivity to reduction of time revisit at 10 days, but it is generally comprised within 3.2 days difference to the baseline (2 times standard deviation across all test beds). Averaging over all macrophyte test beds, the MAE is lower than 1.6 days, and Max_span is under 2.8 days. Among timing metrics tested, EoS is more sensitive to reducing time revisit from 5 to 10 days (MAE = 1.6 days), compared to SoS and PoS (MAE < 1.2 days).

Further reduction of temporal resolution of input time series up to 15 days, near to the nominal 16 day revisit of Landsat 4-8 satellites operationally collecting data all over the globe since 1982, results in differences in TIMESAT output phenology metric up to 6 days across all macrophyte species test beds. Influence on timing metrics is variable across macrophyte test beds investigated, and is generally comprised within 4.8 days difference to the baseline (2 times standard deviation across all test beds). Averaging over all macrophyte test beds, the MAE of 15-

day revisit time series can reach up to 2.8 days, while Max_span peaks at 7.4 days. As with 10-day reduced resolution, EoS is more sensitive (MAE = 2.7 days) than SoS and PoS (MAE < 1.8 days).

Table 5. Influence of temporal resolution of input time series on TIMESAT output metrics (SoS, PoS, EoS) for Mantua lakes system dataset

		Difference *vs*. baseline (Mantua_5d)		
		ΔSoS (days)	**ΔPoS (days)**	**ΔEoS (days)**
Mantua_10d_a	NNs	1.8	-3.8	-3.6
	TNm	-0.3	0.7	2.4
	TNi	-0.7	-0.4	-1.1
	NLv	1.3	1.4	0.2
Mantua_10d_b	NNs	0.9	-0.4	-0.5
	TNm	-2.6	0.5	0.8
	TNi	0.3	-0.1	2.2
	NLv	-0.8	-1.0	-0.5
Mantua_10d	**MAE**	**1.19**	**1.15**	**1.59**
	Max-span	*1.94*	*2.00*	*2.75*
Mantua_15d_a	NNs	1.2	1.7	4.5
	TNm	-2.8	1.3	2.6
	TNi	-0.8	-3.7	-0.9
	NLv	1.0	0.5	3.9
Mantua_15d_b	NNs	-1.2	-4.3	-5.9
	TNm	-2.1	-3.2	-5.3
	TNi	4.0	0.8	-0.1
	NLv	0.3	-0.1	-3.2
Mantua_15d_c	NNs	1.4	-1.3	-1.5
	TNm	-2.0	-0.7	-0.6
	TNi	-1.5	-0.4	0.3
	NLv	-0.7	0.5	-0.2
Mantua_15d	**MAE**	**1.64**	**1.76**	**2.71**
	Max_span	*3.09*	*4.46*	*7.35*

Macrophyte test beds: NNs: *N. nucifera* (Superior Lake); TNm: *T. natans* (Middle Lake); TNi: *T. natans* (Inferior Lake); NLv: *N. lutea* (Vallazza wetland)

5.4.2. Influence of missing acquisitions

Based on baseline results derived from the complete time series at 5-day temporal resolution (Figures 8a, 8b, 8c), five seasonal ranges were identified: i) pre-season (DOY < 100); ii) early season, when most of macrophyte start of season dates occur (100 < DOY < 180); iii) full season,

when peak of vegetative and reproductive phase for macrophyte communities investigated take place (180 < DOY < 250); iv) late season, after plant maturity is reached and senescence develops (250 < DOY < 320); and v) post-season (DOY > 320). These five seasonal ranges were used to interpret results of missing acquisitions influence.

At 5-day revisit (Figure 11a), EoS is the most sensitive parameter to missing a single date of the time series, with a MAE with respect to baseline (complete time series: Mantua_5d dataset) reaching 3.5 days, while PoS and SoS are more robust to missing dates (MAE = 1.7 and 0.8, respectively). Sensitivity is pronounced for NNs test bed (populated by *N. nucifera*), with a maximum difference compared to the full dataset up to 8.3 days for EoS, and up to 4.2 days for PoS (i.e. when DOY 297 date is removed from the time series). The other macrophyte test samples, populated by *T. natans* and *N. lutea* communities, show lower sensitivity to missing acquisitions, with maximum difference to baseline lower than 1.5 days. Key periods for effectively capturing phenology timing from satellite LAI time series are therefore the early season (April-May) for SoS estimation, the late season (September-October) for PoS and EoS estimation, and late to post-season (October-November) for EoS estimation.

At 15-day revisit (Figure 11b), results are generally consistent with what highlighted for 5-day revisit, although with wider score ranges. SoS and EoS are the most sensitive parameters to missing a single date, with a MAE with respect to baseline (complete time series: Mantua_15d_b dataset) around 2.7 days, while PoS is more robust (MAE = 1.5). Again, sensitivity is pronounced for NNs test bed, with a maximum difference compared to the full dataset up to 5.4 days for EoS, and up to 5.1 days for SoS. TNm test bed show high sensitivity to missing dates too, with differences up to 7.9 days for EoS, when dates in late to post-season time are removed from the time series. Sensitivity of timing metrics of TNi are less evident, and those for NLv are still the lower ones (< 2 days). At seasonal range level, key periods at 15-day temporal resolution are the

same as for 5-day revisit.

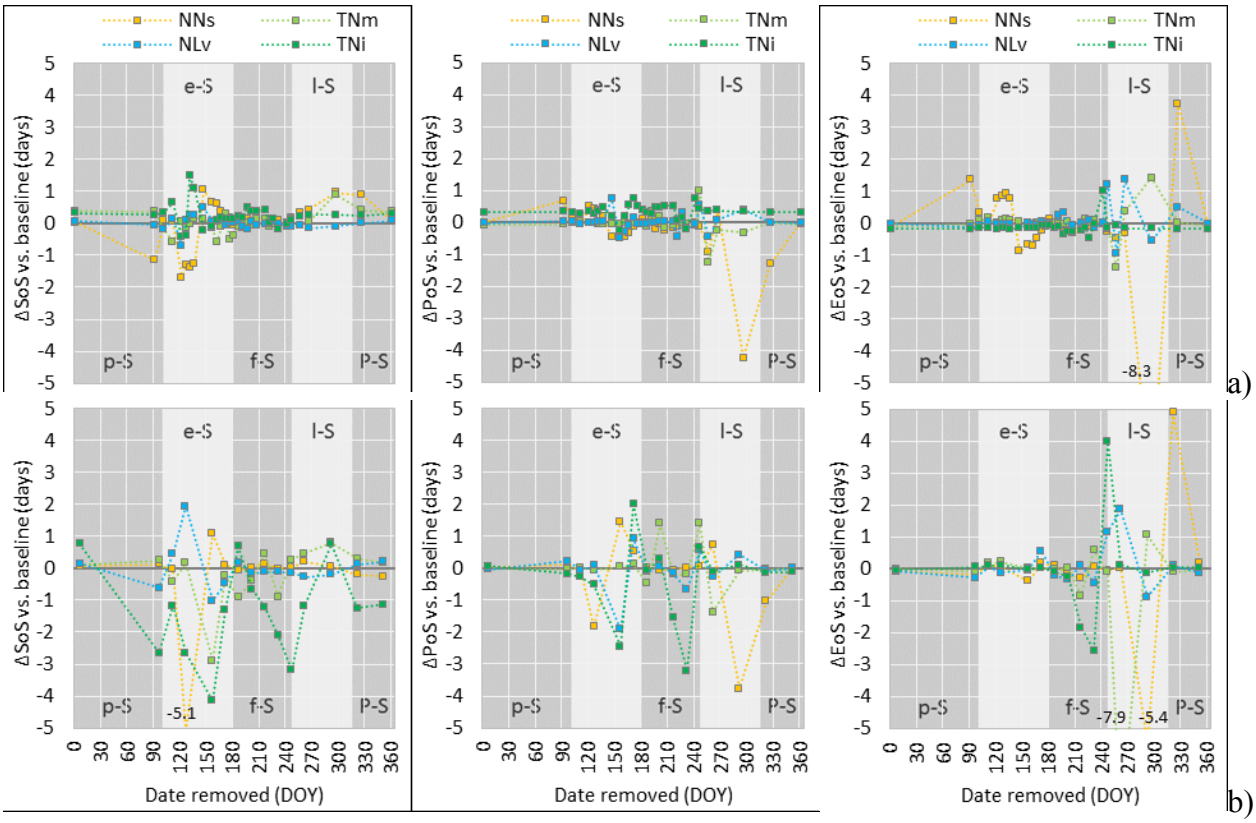

Figure 11. Influence of missing dates in the input time series on TIMESAT output metrics (SoS, PoS, EoS) for Mantua lakes system dataset, at: a) 5 day temporal resolution, and b) 15 day temporal resolution. Seasonal ranges highlighted by different grey colour background: p-S: pre-season; e-S: early season; f-S: full season; l-S: late season; P-S: post-season. Macrophyte test beds: NNs: *N. nucifera* (Superior Lake); TNm: *T. natans* (Middle Lake); TNi: *T. natans* (Inferior Lake); NLv: *N. lutea* (Vallazza wetland)

6. Discussion

6.1.Macrophyte LAI mapping from satellite data

Satellite data coming from different medium resolution platforms (SPOT5, Landsat 7/8, Sentinel-2A) can be integrated into consistent time series of surface spectral reflectance with radiometric mismatch across sensors contained within acceptable levels, with a relative MAE < 0.04 between SPOT5 and Landsat 8 or Sentinel-2A data and an absolute MAE < 0.07 compared to *in situ*

spectra. Compared to EVI2 derived from SPOT5 bands, both Landsat 8 and Sentinel-2A tend to score higher by around 30% in the high end of values. This is probably due to the difference in atmospheric correction algorithm used for the two types of data, MACCS for SPOT5 and ATCOR for Landsat and Sentinel-2, and implies that macrophyte LAI mapped are slightly overestimated in the temporal range not covered by SPOT5 Take5 dataset. Nevertheless, being this range (before April and after September) mostly outside the growing season for macrophytes in temperate areas, the effect on TIMESAT derived phenology metrics is considered minor.

LAI for target macrophyte species (floating, floating-leaved, emergent) was reliably estimated using the semi-empirical regression model based on EVI2, as best performing spectral index: the MAE scored for independent validation data is 0.11 m^2 m^{-2}, with a tendency to underestimation due to index saturation only occurring for LAI > 1.5. This confirms the findings of previous works (Villa et al., 2016; Villa et al., 2017), extending the application feasibility to multispectral platforms.

6.2.Macrophyte seasonal dynamics at the study areas

Seasonal dynamics maps derived using TIMESAT fed with macrophyte LAI time series showed differences in both spatial and temporal patterns across the three study areas, temperate shallow ecosystems inhabited by shared and common macrophyte species.

Nymphaeids – which mainly consist in *N. lutea* and *N. alba* in our study areas, being *N. peltata* present in small scattered patches covering less than 2 ha at maximum (in Lac de Grand-Lieu) – show growing season shifted later by 10-30 days in Fundu Mare Island, compared to Mantua lakes system and Lac de Grand-Lieu, as a possible effect of water level fluctuation observed in the Romanian wetland (Figure 2). Here, the LAI peak value is higher than 1.1, probably due to interference of willow encroachment observed in the *N. alba* beds. In Mantua lakes system,

where nymphaeids cover a small area (< 6% of macrophyte surface) the growing season is the shortest and LAI growth rate slowest, of all study areas. In the Lac de Grand-Lieu, the seasonal dynamic of the nymphaeids can also affect the interpretation of the maps. *N. alba* can have a bimodal development with a first peak of biomass in spring and a second one late in summer or just one single peak of vegetation development (Paillisson and Marion, 2006). This dynamic depends on the years and, probably varies locally within the lake.

Water chestnut (*T. natans*), the other species common to all three study areas, shows the highest on site variability in timing metrics (SoS, PoS, EoS) in Mantua lakes system, where different sub-systems link to spatially heterogeneous phenology. Here, *T. natans* beds have adapted well to different environmental conditions of the lakes, becoming dominant in all lakes except the Superior Lake and covering almost 50% of total macrophyte area.

On average, these species start growing later in Mantua lakes system and reaches peak LAI values greater than 1.20 m^2 m^{-2}. Such anomalous scores for a floating species are due to the mixture with duckweed (lemnoids, such as *Lemna* ssp., *Spirodela polyrhiza*), coexisting with *T. natans* in Middle and Inferior lakes stands in full summer (July and August) and increasing the total leaf area per unit surface.

In the Lac de Grand-Lieu, where *T. natans* covers only a small area (< 5% of macrophyte surface) and is outcompeted by nymphaeids, growing season peaks and ends earlier than in the other two sites, and the plant density reached is by far the lowest, with LAI ~ 0.5-0.6 m^2 m^{-2}. The species has been in decline for the last forty years in Grand-Lieu, but the hydro-meteorological conditions in 2015 spring may have exacerbated the trend: a late flood at beginning of May rose lake level by 40 cm in 5 days, with a possible effect on *T. natans* germination and growth.

The allochthonous lotus flower (*N. nucifera*) is present only in Mantua lakes system, where it was introduced in 1921. The seasonal dynamics maps clearly show the distinct invasiveness traits

of this species, characterized by fast growth (0.03-0.05 m^2 m^{-2} d^{-1}, from May to June), long persistence (EoS in October-November), high density and coverage (LAI up to 1.7 m^2 m^{-2}). These characteristics can easily explain how the autochthonous species (*T. natans* and *N. lutea*) were outcompeted by *N. nucifera* during the last century in Mantua lakes system, bringing to a situation where lotus flower almost completely dominates Superior Lake, covering up to 45% of total macrophyte surface in the area, and needs to be managed by cutting on a yearly basis (Villa et al., 2017). This is a crucial point considering the very high number of allochthonous species spread in aquatic ecosystems, especially in temperate regions (Hussner, 2012; Bolpagni et al., 2013). They represent one of the most critical factors affecting the survival of autochthonous aquatic species and habitats (Gallardo et al., 2016).

In this study, the time for the start of the season was defined as the time when the macrophytes overpassed 25% of peak LAI, based on observation of target macrophyte species. This may be different, however, in presence of diffused willow encroachment, as we found at Fundu Mare Island. Young *Salix* spp., partly inundated during the spring, developed only later in the season depending on the decreasing water levels, thus affecting the LAI mapped for macrophyte patches subject to encroachment.

Riparian vegetation composition, structure and vigour responds rapidly to hydrological regime changes (e.g. Merritt et al., 2010; Johnson, 2000; Loheide and Booth, 2011). This study showed that seasonal dynamics metrics derived from TIMESAT output parameters, in particular PoS and EoS, could be related to specific vegetation community types. Vegetation zoning in floodplains, such as Fundu Mare Island, is closely related to the flooding duration and the mean summer water level (Ellenberg, 1996).

The use of medium resolution satellite data offers therefore new opportunities for monitoring and studying on-going vegetation changes, for example the encroachment of willows in zones that

were earlier mapped as aquatic habitats. Moreover, the description of vegetation seasonal dynamics in terms of LAI, which can be used for the parameterization of flow resistance of floodplain vegetation (Aberle and Järvelä, 2013), may support the application of hydrodynamic models for flow and sediment transport for complex riparian environments.

6.3.Influence of satellite data variables on phenology metrics

The assessment of the satellite data characteristics on macrophyte seasonal dynamics derived from TIMESAT brought to interesting results in terms of operational requirements and the error level one can expect when input time series is sub-optimal. The effect of cloud cover threshold setting is contained within maximum 2-day difference for the estimation of SoS, and even less for PoS and EoS. Temporal resolution is more decisive, reaching 2.8 and 7.4 maximum difference in EoS estimation, when time revisit of input time series is reduced from nominal 5 days to 10 and 15 days (similar to Landsat series revisit), respectively. The difference is less severe from SoS and PoS, for which the estimation bias can reach 1.8 and 3.1 days maximum, respectively. Based on these results, Landsat 4-8 data, acquired consistently from 1982 all over the globe, could be used for mapping phenology timing of macrophytes in retrospective way, with and error level around 2-3 days for SoS and PoS.

The analysis of influence of missing acquisitions, e.g. covered by clouds, highlights once again that EoS is the most sensitive timing parameter, with average difference of 3.5 days and maximum of 8.3 days, when satellite scenes are missing in the late season (from mid-September to mid-November). Differences for SoS and PoS are contained within 2 days and 5 days, respectively. This is especially relevant for *N. nucifera*, while timing metric differences for *T. natans* and *N. lutea* are generally lower (< 1.5 days).

7. Conclusions

We investigated the capabilities of time series of multisource satellite data with 5 to 10 day revisit for mapping LAI and seasonal phenological metrics of floating and emergent macrophytes over three shallow freshwater systems in continental Europe. Macrophyte LAI maps were derived from semi-empirical regression modelling, based on the best performing spectral index (EVI2), with an error level around 0.1 m^2 m^{-2}, calculated from independent validation data. Seasonal dynamics of macrophytes were mapped from phenology metric computed using TIMESAT code, highlighting spatial-wise patterns and species-dependent variability for the year 2015 across the three study areas, which were related to the environmental characteristics of each area in terms of ecological, hydrological and meteorological conditions. Moreover, the influence of TIMESAT input data parameters such as cloud cover thresholding, temporal resolution and chance of missing acquisitions have been assessed by comparing phenology timing metrics (SoS, PoS and EoS) outputs with respect to a baseline, i.e. complete time series of LAI maps at 5 day revisit and 95% maximum cloud cover.

Our findings demonstrate that dense time series of different medium resolution satellite data (Landsat, SPOT, Sentinel-2) can be integrated to provide consistent maps of macrophyte LAI and their seasonal dynamics, although some criticality remain dealing with atmospheric correction using different algorithms and correspondence of TIMESAT derived metrics with actual phenological phases of different species. The use of satellite data for mapping macrophyte dynamics in quantitative way at local to regional scales offers new possibilities for the monitoring of restoration and conservation actions in shallow aquatic ecosystems, i.e. the effect of measures affecting the hydrological conditions as well as the rapid changes that characterized the intra- and inter-seasonal macrophyte dynamicity. Furthermore, the results described confirm

the effectiveness of remote sensing techniques in investigating driving factors of potential allochthonous species establishment, and in particular the competition of autochthonous vs. allochthonous species.

Acknowledgements

This study has received funding from the European Community's 7th Framework Programme, under project INFORM [grant no. 606865]. SPOT5 data have been acquired in the framework of SPOT5 (Take5) initiative, sponsored by CNES and ESA, and the time series covering Mantua lakes system was proposed within the MacroSentinel project [ESA project ID 29146].

The monitoring of the floating macrophytes in Lac de Grand-Lieu was supported by the Regional Directorate of Environment (DREAL) of Pays de la Loire, the regional Council of Pays de la Loire and Loire-Atlantique Federation of Hunters.

The investigations at Fundu Mare Island were funded by the European Economic Area (EEA) project "Restoration of the aquatic and terrestrial ecosystems of Fundu Mare Island" [grant no. RO02-0008] with financial contributions from Norway and Romania, and the support of the Natural Park Administration of the Small Wetland of Braila.

The authors thank Ilaria Cazzaniga (CNR-IREA) for her help during fieldwork in Mantua lakes system.

References

Aberle J, Järvelä J (2013) Flow resistance of emergent rigid and flexible floodplain vegetation. J Hydraul Res 51:33–45

Alahuhta, J., Heino, J., & Luoto, M. (2011). Climate change and the future distributions of aquatic macrophytes across boreal catchments. Journal of Biogeography, 38(2), 383-393.

Bolpagni, R., Bartoli, M., & Viaroli, P. (2013). Species and functional plant diversity in a heavily impacted riverscape: Implications for threatened hydro-hygrophilous flora conservation. Limnologica, 43, 230-238.

Bolpagni, R., Bresciani, M., Laini, A., Pinardi, M., Matta, E., Ampe, E.M., Giardino, C., Viaroli, P., & Bartoli M. (2014). Remote sensing of phytoplankton-macrophyte coexistence in shallow hypereutrophic fluvial lakes. Hydrobiologia 737: 67-76.

Broge, N. H., & Leblanc, E. (2001). Comparing prediction power and stability of broadband and hyperspectral vegetation indices for estimation of green leaf area index and canopy chlorophyll density. Remote sensing of environment, 76(2), 156-172.

Cleland, E. E., Chuine, I., Menzel, A., Mooney, H. A., & Schwartz, M. D. (2007). Shifting plant phenology in response to global change. Trends in Ecology & Evolution, 22(7), 357−365.

Dai, X., & Khorram, S. (1998). The effects of image misregistration on the accuracy of remotely sensed change detection. IEEE Transactions on Geoscience and Remote sensing, 36(5), 1566-1577.

Drusch, M., Del Bello, U., Carlier, S., Colin, O., Fernandez, V., Gascon, F., ... & Meygret, A. (2012). Sentinel-2: ESA's optical high-resolution mission for GMES operational services. Remote Sensing of Environment, 120, 25-36.

Dupont P. (2003). L'évolution de la flore et de la végétation du lac de Grand-Lieu et de ses ceintures. Situation actuelle. Problèmes de conservation et de gestion. Bull. Soc. Bot. Centre-ouest. Nouvelle série, 34, 3-64.

Eklundh, L. & Jönsson, P. (2015). Timesat 3.2 Software Manual, Lund and Malmö University, Sweden. http://web.nateko.lu.se/timesat/docs/TIMESAT32_software_manual.pdf

Ellenberg, H. 1996. Vegetation Mitteleuropas mit den Alpen. 5. Auflage. Ulmer Verlag.

Fensholt, R., Horion, S., Tagesson, T., Ehammer, A., Grogan, K., Tian, F., Huber, S., Verbesselt, J., Prince, S.D., Tucker, C.J. and Rasmussen, K., 2015. Assessment of Vegetation Trends in Drylands from Time Series of Earth Observation Data. In Remote Sensing Time Series (pp. 159-182). Springer International Publishing.

Fisher, J. I., & Mustard, J. F. (2007). Cross-scalar satellite phenology from ground, Landsat, and MODIS data. Remote Sensing of Environment, 109(3), 261-273.

Fisher, J. I., Richardson, A. D., & Mustard, J. F. (2007). Phenology model from surface meteorology does not capture satellite-based greenup estimations. Global Change Biology, 13(3), 707-721.

Gao, F., Morisette, J. T., Wolfe, R. E., Ederer, G., Pedelty, J., Masuoka, E., ... & Nightingale, J. (2008). An algorithm to produce temporally and spatially continuous MODIS-LAI time series.

IEEE Geoscience and Remote Sensing Letters, 5(1), 60-64.

Gallardo, B., Clavero, M., Sánchez, M. I., & Vilà, M. (2016). Global ecological impacts of invasive species in aquatic ecosystems. Global Change Biology, 22(1), 151-163.

Gillier J.M. & Reeber S. (2016). Suivi spatial de la zone centrale du Lac de Grand-Lieu en 2015. DREAL Pays de la Loire, Région Pays de la Loire, Syndicat de Bassin Versant de Grand-Lieu, SNPN, Fédération Départementale des Chasseurs de Loire-Atlantique. 24 p.

Gitelson, A., & Merzlyak, M. N. (1994). Quantitative estimation of chlorophyll-a using reflectance spectra: Experiments with autumn chestnut and maple leaves. Journal of Photochemistry and Photobiology B: Biology, 22(3), 247-252.

Haboudane, D., Miller, J. R., Pattey, E., Zarco-Tejada, P. J., & Strachan, I. B. (2004). Hyperspectral vegetation indices and novel algorithms for predicting green LAI of crop canopies: Modeling and validation in the context of precision agriculture. Remote sensing of environment, 90(3), 337-352.

Hagolle, O., Huc, M., Villa Pascual, D., & Dedieu, G. (2015). A multi-temporal and multi-spectral method to estimate aerosol optical thickness over land, for the atmospheric correction of Formosat-2, Landsat, Venμs and Sentinel-2 images. Remote Sensing, 7(3), 2668-2691.

Haury J., Noël F., Bozec M., Coudreuse J., Guil J., Marrel G., Maisonneuve J.L. & Damien J.P. (2011). Importance of Ludwigia grandiora as invasive weed on meadows and pastures in Western France. 3rd International Symposium on Weeds and Invasive Plants, Oct 2011, Ascona (CH), Switzerland.

Hestir, E. L., Brando, V. E., Bresciani, M., Giardino, C., Matta, E., Villa, P., & Dekker, A. G. (2015). Measuring freshwater aquatic ecosystems: The need for a hyperspectral global mapping satellite mission. Remote Sensing of Environment, 167, 181-195.

Huete, A. R. (1988). A soil-adjusted vegetation index (SAVI). Remote sensing of environment, 25(3), 295-309.

Hussner, A. (2012). Alien aquatic plant species in European countries. Weed Research, 52(4), 297-306.

Jenkins, J. P., Braswell, B. H., Frolking, S. E., & Aber, J. D. (2002). Detecting and predicting spatial and interannual patterns of temperate forest springtime phenology in the eastern US. Geophysical Research Letters, 29(24).

Jiang, Z., Huete, A. R., Didan, K., & Miura, T. (2008). Development of a two-band enhanced vegetation index without a blue band. Remote Sensing of Environment, 112(10), 3833-3845.

Johnson, W.C. 2000. Tree recruitment and survival in rivers: influence of hydrological processes. Hydrological Process 14(16-17): 3015-3074.

Jönsson, P. & Eklundh, L. (2002). Seasonality extraction and noise removal by function fitting to time-series of satellite sensor data, IEEE Transactions of Geoscience and Remote Sensing, 40, No 8, 1824 – 1832.

Jönsson, P., & Eklundh, L. (2004). TIMESAT—a program for analyzing time-series of satellite sensor data. Computers & Geosciences, 30(8), 833-845.

Karnieli, A., Kaufman, Y. J., Remer, L., & Wald, A. (2001). AFRI—Aerosol free vegetation

index. Remote Sensing of Environment, 77(1), 10-21.

Kaufman, Y. J., Tanré, D., Remer, L. A., Vermote, E. F., Chu, A., & Holben, B. N. (1997). Operational remote sensing of tropospheric aerosol over land from EOS moderate resolution imaging spectroradiometer. Journal of Geophysical Research: Atmospheres, 102(D14), 17051–17067.

Laben, C. A., & Brower, B. V. (2000). U.S. Patent No. 6,011,875. Washington, DC: U.S. Patent and Trademark Office.

Le Bail J. (2008). La flore des characées du Lac de Grand-Lieu et ses abords (Loire Atlantique): observations anciennes et état actuel. E.R.I.C.A., 21, p. 45-52.

Li, Z., He, L., Zhang, H., Urrutia-Cordero, P., Ekvall, M.K., Hollander, J. and Hansson, L.A., 2017. Climate warming and heat waves affect reproductive strategies and interactions between submerged macrophytes. Global change biology, 23(1), pp.108-116.

Loheide, S.P. & Booth, E.G. 2011. Effects of changing channel morphology on vegetation, groundwater, and soil moisture regimes in groundwater-dependent ecosystems. Geomorphology 126(3-4): 364-376.

Luo, J., Li, X., Ma, R., Li, F., Duan, H., Hu, W., Qin, B. and Huang, W., 2016. Applying remote sensing techniques to monitoring seasonal and interannual changes of aquatic vegetation in Taihu Lake, China. Ecological Indicators, 60, pp.503-513.

Lymburner, L., Beggs, P. J., & Jacobson, C. R. (2000). Estimation of canopy-average surface-specific leaf area using Landsat TM data. Photogrammetric Engineering and Remote Sensing, 66(2), 183-192.

Malthus, T. J. (2017). Bio-optical Modeling and Remote Sensing of Aquatic Macrophytes. Bio-optical Modeling and Remote Sensing of Inland Waters, 263.

Marion L. & Marion P. (1975). Contribution à l'étude écologique du lac de Grand-Lieu. Bulletin de la Société des Sciences Naturelles de l'Ouest de la France, 611 p.

Maxwell, S. K., Schmidt, G. L., & Storey, J. C. (2007). A multi-scale segmentation approach to filling gaps in Landsat ETM+ SLC-off images. International Journal of Remote Sensing, 28(23), 5339-5356.

Merritt, D.M., Scott, M.L., LeRoy, Poff N., Auble, G.T., Lytle, D.A. 2010. Theory, methods and tools for determining environmental flows for riparian vegetation: riparian vegetation-flow response guilds. Freshwater Biology 55(1): 206-225.

Netten, J. J., Van Zuidam, J., Kosten, S., & Peeters, E. T. (2011). Differential response to climatic variation of free-floating and submerged macrophytes in ditches. Freshwater Biology, 56(9), 1761-1768.

Paillisson J.M., Marion L. (2006). Can small water level fluctuations affect the biomass of Nymphaea alba in large lakes? Aquatic Botany, 84, 259-266.

Peel MC, Finlayson BL, McMahon TA (2007) Updated world map of the Köppen-Geiger climate classification. Hydrol Earth Syst Sci 11:1633–1644

Peeters, E. T., Zuidam, J. P., Zuidam, B. G., Nes, E. H., Kosten, S., Heuts, P. G., ... & Scheffer, M. (2013). Changing weather conditions and floating plants in temperate drainage

ditches. Journal of Applied Ecology, 50(3), 585-593.

Pinardi M, Bartoli M, Longhi D, Viaroli P, 2011. Net autotrophy in a fluvial lake: the relative role of phytoplankton and floating-leaved macrophytes. Aquat. Sci. 73(3):389-403.

Pinardi, M., Fenocchi, A., Giardino, C., Sibilla, S., Bartoli, M., & Bresciani, M. (2015). Assessing potential algal blooms in a shallow fluvial lake by combining hydrodynamic modelling and remote-sensed images. Water, 7(5), 1921-1942.

Reed, B. C., Brown, J. F., VanderZee, D., Loveland, T. R., Merchant, J. W., & Ohlen, D. O. (1994). Measuring phenological variability from satellite imagery. Journal of vegetation science, 5(5), 703-714.

Reed, B.C., 2006. Trend analysis of time-series phenology of North America derived from satellite data. GIScience & Remote Sensing, 43(1), pp.24-38.

Richardson, A. D., Keenan, T. F., Migliavacca, M., Ryu, Y., Sonnentag, O., & Toomey, M. (2013). Climate change, phenology, and phenological control of vegetation feedbacks to the climate system. Agricultural and Forest Meteorology, 169, 156-173.

Richter R., & D. Schläpfer (2011). Atmospheric/Topographic Correction for Satellite Imagery, DLR report DLR-IB 565-02/11, Wessling (D), pp 202.

Rouse Jr, J., Haas, R. H., Schell, J. A., & Deering, D. W. (1974). Monitoring vegetation systems in the Great Plains with ERTS. NASA special publication, 351, 309.

Sletvold N., Ågren J. 2015. Climate-dependent costs of reproduction: Survival and fecundity costs decline with length of the growing seasonand summer temperature. Ecology Letters 18: 357-364. DOI: 10.1111/ele.12417

SWB 2015. Database and information materials of the “Par-cul Natural Balta Mica a Brailei”. http://bio.geoportal-mediu.ro/viewer/bmb/, accessed in September 2015.

Tan, B., Morisette, J. T., Wolfe, R. E., Gao, F., Ederer, G. A., Nightingale, J., & Pedelty, J. A. (2011). An enhanced TIMESAT algorithm for estimating vegetation phenology metrics from MODIS data. IEEE Journal of Selected Topics in Applied Earth Observations and Remote Sensing, 4(2), 361-371.

Tian Y.C., Zhu Y., Cao W.X. (2005). Monitoring soluble sugar, total nitrogen & its ratio in wheat leaves with canopy spectral reflectance. Acta Agronomica sinica, 31: 355-360.

Villa, P., Boschetti, M., Morse, J. L., & Politte, N. (2012). A multitemporal analysis of tsunami impact on coastal vegetation using remote sensing: a case study on Koh Phra Thong Island, Thailand. Natural hazards, 64(1), 667-689.

Villa, P., Bresciani, M., Bolpagni, R., Pinardi, M., & Giardino, C. (2015). A rule-based approach for mapping macrophyte communities using multi-temporal aquatic vegetation indices. Remote Sensing of Environment, 171, 218-233.

Villa, P., Mousivand, A., & Bresciani, M. (2014). Aquatic vegetation indices assessment through radiative transfer modeling and linear mixture simulation. International Journal of Applied Earth Observation and Geoinformation, 30, 113-127.

Villa, P., Pinardi, M., Tóth, V. R., Hunter, P. D., Bolpagni, R., & Bresciani, M. (2017). Remote sensing of macrophyte morphological traits: implications for the management of shallow

lakes. Journal of Limnology, 76(s1): 109-126.

Wang L., Dronova I., Gong P., Yang W., Li Y. Liu, Q. 2012. A new time series vegetation-water index of phenological-hydrological trait across species and functional types for Poyang Lake wetland ecosystem. Remote Sensing of Environment, 125: 49-63.

White, M. A., & Nemani, A. R. (2003). Canopy duration has little influence on annual carbon storage in the deciduous broad leaf forest. Global Change Biology, 9(7), 967−972.

Wolkovich, E. M., & Cleland, E. E. (2011). The phenology of plant invasions: a community ecology perspective. Frontiers in Ecology and the Environment, 9(5), 287-294.

Yang, Y., Guan, H., Shen, M., Liang, W. and Jiang, L., 2015. Changes in autumn vegetation dormancy onset date and the climate controls across temperate ecosystems in China from 1982 to 2010. Global change biology, 21(2), pp.652-665.

Zhang X., Odgaard R., Olesen B., Lauridsen T.L., Liboriussen L.,Søndergaard M., Liu Z., Jeppesen E. 2015. Warming shows differential effects on late-season growth and competitive capacity of Elodea canadensis and Potamogeton crispus in shallow lakes. Inland Waters, 5(4): 421-432. DOI: 10.5268/IW-5.4.830

Zhang, X., Friedl, M. A., Schaaf, C. B., Strahler, A. H., Hodges, J. C., Gao, F., ... & Huete, A. (2003). Monitoring vegetation phenology using MODIS. Remote sensing of environment, 84(3), 471-475.

Zinke P, Aberle J, Nedelcut F (2016) Vegetation changes at “Fundu Mare Island” in the Inner Danube Delta near Brăila (Romania). River Flow 2016 2174–2181